A *Mycobacterium tuberculosis* effector targets mitochondrion, controls energy metabolism and limits cytochrome c exit.

Marianne Martin[1], Angelique deVisch[4], Yves-Marie Boudehen[2], Philippe Barthe[4], Claude Gutierrez[2], Obolbek Turapov[3], Talip Aydogan[1], Laurène Heriaud[4], Jerome Gracy[4], Olivier Neyrolles[2], Galina V. Mukamolova[3], François Letourneur[1]*, Martin Cohen-Gonsaud[4]*

[1] Laboratory of Pathogen Host Interactions (LPHI), CNRS, University of Montpellier, France.
[2] Institut de Pharmacologie et de Biologie Structurale, Université de Toulouse CNRS, UPS, Toulouse, France.
[3] Leicester Tuberculosis Research Group, Department of Respiratory Sciences, University of Leicester, UK.
[4] Centre de Biochimie Structurale, CNRS, INSERM, Université de Montpellier, France.

* Corresponding authors

Abstract

Host metabolism reprogramming is a key feature of *Mycobacterium tuberculosis* (*Mtb*) infection that enables the survival of this pathogen within phagocytic cells and modulates the immune response facilitating the spread of the tuberculosis disease. Here, we demonstrate that a previously uncharacterized secreted protein from *Mtb*, Rv1813c manipulates the host metabolism by targeting mitochondria. When expressed in eukaryotic cells, the protein is delivered to the mitochondrial intermembrane space and promotes the enhancement of host ATP production by boosting the oxidative phosphorylation metabolic pathway. Furthermore, the release of cytochrome c from mitochondria, an early apoptotic event in response to short-term oxidative stress, is delayed in Rv1813c expressing cells. This study reveals a novel class of mitochondria targeting effectors from *Mtb* which might participate in host cells metabolic reprogramming and apoptosis control during *Mtb* infections.

Introduction

Mycobacterium tuberculosis (*Mtb*) encodes secreted virulence factors contributing to its successful infection of host cells and its ability to actively replicate inside the phagosome (Hmama et al., 2015) (Winden et al., 2019). After phagocytosis, *Mtb* blocks phagosomal maturation, escapes phagosomes and subverts the host immune response. Several virulence factors (*e.g.* proteins, lipids) have been already described to mediate such mechanisms, but corruption of host cell defenses is clearly

multifactorial (Nicholson et al., 2021). It is estimated that over 20% of bacterial proteins have functions outside the bacterial cytoplasm and are exported to their designated locations by protein export systems (Kostakioti et al., 2005). Identification of secreted proteins remains a challenging task (Målen et al., 2007; de Souza et al., 2011; Albrethsen et al., 2013). The comparison of *Mtb* secreted proteins reported in various proteomic studies revealed only a small number of proteins consistently identified (Tucci et al., 2020). As experiments were made in various culture conditions, it is not surprising that secretion patterns differ from one experiment to another. Furthermore, the host cell environment also plays an important role in defining the secretion pattern, as recently revealed by studies focusing on the identification of secreted proteins during infection (Perkowski et al., 2017; Penn et al., 2018). To get a broader view on the *Mtb* secretome, we used multidisciplinary approaches including bioinformatics, structural and biochemical techniques, and cellular biology analyzes. We identified putative *Mtb* secreted proteins using proteins primary sequence analysis combined with structure modelling. Among the selected targets, we studied the protein coded by the *rv1813c* gene which is only present in mycobacterial pathogens. The Rv1813c protein has been used as vaccine adjuvant (Bertholet et al., 2008) and displays immunogenicity properties (Liang et al., 2019). Rv1813c expression was reported to be MprA and DosR regulated (Bretl et al., 2012) and *Mtb* ΔRv1813c mutant was attenuated in the low-dose aerosol model of murine tuberculosis (Bretl et al., 2012).

In this paper, we describe molecular and functional analyzes of this protein. We showed that Rv1813c defines a new class of effectors, with an original fold, addressed to mitochondria. Mitochondrion plays critical functions not only supplying cells with energy but also contributing to several cellular mechanisms including cell cycle, apoptosis, and signaling pathways. Metabolism modulation dictates macrophage function and subsequent *Mtb* infection progression. Here, we demonstrate that Rv1813c affects some mitochondrial metabolic functions and cellular responses to oxidative stress. These results suggest that Rv1813c might play regulatory roles in the metabolic and apoptotic responses occurring in *Mtb* infected macrophages.

Results

Bioinformatic analysis of *Mtb* genome for identification of secreted proteins

Mtb possesses at least three different secretion systems using distinct secretion determinants (structural and/or motif-based) present on transported proteins (Feltcher et al., 2010). To predict secreted proteins *in silico*, we analyzed the predicted *Mtb* H37Rv proteome using an in-house Protein Analysis Toolkit (PAT) (Gracy and Chiche, 2005). First, SignalP v4.1 and PredTAT softwares were used to predict the presence of known signal peptides and/or structural features necessary for secretion. In addition, transmembrane segments were inferred using either Uniprot annotations or the TmHMM prediction software. The number of predicted transmembrane segments and the

position of the last transmembrane segment were also manually examined to identify signals potentially missed by the other methods. To search for potential T7SS-mediated secreted proteins, we first performed helix structure prediction of each protein using Psipred (McGuffin et al., 2000), and then searched for the YxxxD/E motif in between the characteristic two helices (Daleke et al., 2012). These data were compared with various proteomic data and model databases (ModBase, Interpro, GO). Among the proteins identified here as potentially secreted, we studied Rv1813c, a 143 amino-acid protein with a predicted folded domain of unknown function.

Rv1813c protein sequence features and secretion

Primary sequence analysis of the Rv1813c protein unambiguously identified a potential signal sequence (residues 1 to 28) with an upstream arginine repeat (residues 6-8) indicating that the protein could be exported by the Tat export system (**Fig. 1A**). Consistent with its genuine export signal, Rv1813c has been identified in one culture filtrate proteome (Tucci et al., 2020), but surprisingly is absent in three others published secretomes (Malen et al., 2007; de Souza et al., 2011; Albrethsen et al., 2013). Conversely, Western blot analysis of *Mtb* culture filtrates using a specific antibody here confirmed that Rv1813c is secreted during active growth in culture medium (**Supplementary Fig. S1**). Rv1813c homologous proteins are mostly found in Actinobacteria (*Mycobacterium*, *Nocardia* and *Streptomyces* genera). In addition to *Mtb*, the protein is present in various mycobacteria including *Mycobacterium marinum* (*Mmar*), *Mycobacterium avium*, *Mycobacterium ulcerans* and *Mycobacterium abscessus*. Multiple paralogues exist within the same bacteria. For instance, *Mtb* possesses only one orthologue (Rv1269c), whereas *Mmar* harbors three paralogues (MMAR_1426, MMAR_2533 and MMAR_4153). Remarkably, Rv1269c has been detected in all culture filtrates proteomes published so far (Malen et al., 2007; de Souza et al., 2011; Albrethsen et al., 2013). Therefore, the secretion in culture medium might be a common feature of Rv1813c homologous proteins. The sequence similarity between these various proteins is high (between 45 to 70%), with a lower sequence identity for the N-terminal part (residues 28-54 for Rv1813c) of the protein (**Fig. 1A**). Four cysteine residues are present and conserved. The last four amino acid residues (^{140}WACN^{143}) composed a strictly conserved motif in all Rv1813c homologous proteins that includes one of the conserved cysteines. Fold-recognition and modelling server @TOME2 previously used in many studies for protein function identification even at low sequence identity (Turapov et al., 2014) failed to identify any close or distant Rv1813c structural homologues.

Rv1813c defines a new protein family and a unique protein fold

The Rv1813c-coding sequence without the first codons corresponding to the protein signal peptide (residues 1 to 27) was cloned into an *Escherichia coli* expression vector. The protein was overexpressed as inclusion bodies, purified and refolded. The purified protein was used for multidimensional NMR experiments. Preliminary examination of [1H,15N]-HSQC spectrum revealed that 30

residues were unfolded (**Supplementary Fig. S2**). A full multi-dimensional NMR study led to the protein three-dimensional structure resolution (**Fig. 1B, Supplementary Table S1**). Structure resolution demonstrated that the residues 28 to 57 were unfolded and that the protein possessed a 86 residues folded domain at its carboxyl terminus. This domain is composed of two duplicate lobes facing each other, and each lobe comprises a series of three *ß*-strands with a hydrophobic surface and an *α*-helix (*ß/ß/α/ß*). The four conserved cysteines are engaged in two disulfide bonds located in different parts of each lobe. The proteins from the family defined by the Rv1813c sequence (Pfam domain: DUF4189) contain a conserved WACN motif (Trp-Ala-Cys-Asn residues) with the cysteine engaged in a disulfide bond linking the strands *ß*6 and *ß*4, while its tryptophan is solvent-exposed as well as the second tryptophan (Trp140) in Rv1813c. In addition to protein folding and stability properties, these solvent-accessible tryptophan residues might be functionally important for Rv1813c, contributing either to an hypothetic Rv1813c active site or to interactions with other ligands as classically described for solvent-exposed residues. The overall structure defines a previously undescribed fold as both Dali (Holm and Rosenström, 2010) and FATCAT (Ye and Godzik, 2004) servers failed to detect any structural homologues. Consequently, sequence and structure comparison analysis did not bring any indication on the potential biological function of the Rv1813c protein family.

Rv1813c is addressed to mitochondria in *Dictyostelium* cells.

To assess the function of Rv1813c in host cells, we first used the amoeba *Dictyostelium discoideum*. This professional phagocyte is amenable to biochemical, cell biological and genetic approaches, and has proved to be an advantageous host cell model to analyze the virulence of several pathogenic bacteria (Steinert, 2011; Müller-Taubenberger et al., 2013). Furthermore, the intracellular replication of *Mmar* has been extensively studied in *D. discoideum* and shows similarity to *Mtb* replication in macrophages (Cardenal-Muñoz et al., 2017), indicating that comparable molecular mechanisms are at play in infected *D. discoideum* and mammalian cells. We first analyzed the intracellular localization of Rv1813c when overexpressed in *D. discoideum* (ectopic expression). Though protein expression levels might differ from what is encountered during *Mtb* infection, ectopic expression allows the advantageous analysis of individual secreted mycobacterial proteins without the potentially complexity brought by other bacteria effectors. Hence, this unphysiological expression of Rv1813c serves as a first step towards the biological characterization of this protein and might give some hints on its potential function(s) during *Mtb* infections.

Rv1813c deleted of its predicted signal peptide (first 27 amino acid residues) was tagged with a myc epitope at its N-terminus (myc-Rv1813c_P28-N143*,* here after referred to as myc-Rv1813c) and stably expressed in *D. discoideum.* Confocal microscopy analysis revealed colocalization in ring like structures of myc-Rv1813*c* coinciding with a mitochondrial outer membrane protein, Mitoporin (Troll et al., 1992) **(Fig. 2A).** Mitochondrial targeting was also observed in cells expressing

146 Rv1813c tagged at the C-terminus (Rv1813c-myc) but was lost when Rv1813c was fused to GFP
147 (**Supplementary Fig. S3A**). This specific targeting was independent of the added myc-tag as stain-
148 ing with an anti-Rv1813c polyclonal antibody of untagged Rv1813c showed identical results (**Sup-**
149 **plementary Fig. S3B**). Mitoporin staining patterns were similarly observed in both parental (Ax2)
150 and Rv1813c transfected cells (**Supplementary Fig. S3B, S3C**) excluding gross mitochondrial mor-
151 phological defects induced by Rv1813c expression in *D. discoideum*. In cells labeled with mito-
152 tracker deep red, a specific dye accumulating inside mitochondria, myc-Rv1813c surrounded la-
153 beled mitochondria and was mostly excluded from internal structures (**Fig. 2B**). This result sug-
154 gested that Rv1813c might be attached either to the internal or the cytosolic sides of mitochondrial
155 outer membranes. Interestingly, deletion of the unfolded N-terminus region of Rv1813c (deletion of
156 residues 28 to 48; myc-Rv1813c_49-143) had no effect on Rv1813c localization whereas Rv1813c
157 deprived of the folded region (deletion of residues 57 to 143; myc-Rv1813c_28-56) was not trans-
158 ported to mitochondria (**Fig. 2C**). Thus, the Rv1813c folded domain, which does not contain any
159 known mitochondrial targeting signals, was sufficient to specifically direct this protein to mitochon-
160 drial outer membranes, whereas the unfolded N-terminus region appeared to be dispensable for
161 Rv1813c targeting to mitochondria.
162
163 **Rv1813c homologues are addressed to mitochondria in *Dictyostelium* cells.**
164 Intracellular localization studies were next extended to members of the Rv1813c family in *Mtb* and
165 *Mmar* in the amoeba. All these proteins were detected in mitochondria, however some Rv1813c-
166 like proteins affected mitochondria morphology. Whereas the overexpression of Rv1813c *Mmar*
167 orthologs (MMA_1426 and MMA_2533) did not induce any apparent morphological defects in mi-
168 tochondria, cells expressing Rv1269c or its *Mmar* ortholog MMA_4153 displayed mitochondria with
169 aberrant shapes and sizes (**Supplementary Fig. S3D**). In addition to mitochondria, MMA_4153 also
170 localized to the cytosol. Taken together, these results indicated that mitochondrial targeting in *D.*
171 *discoideum* is a characteristic feature of the Rv1813c family, and for some members, this localiza-
172 tion leads to defective mitochondrial morphology.
173
174 **Rv1813c resides in the mitochondrial intermembrane space**
175 Mitochondria are composed of two membranes, the outer and inner membranes, separated by an
176 intermembrane space (IMS**) (Fig. 3A)**. To determine more precisely the localization of Rv1813c
177 within these submitochondrial compartments in *D. discoideum*, we next applied a biochemical ap-
178 proach. First, mitochondria enriched fractions (here after referred to as mitochondria) were obtained
179 by subcellular fractionation (see scheme **Fig. 3B**). As expected, Rv1813c was recovered from the
180 mitochondrial fraction confirmed by Mitoporin enrichment (**Fig. 3C**). Next, Triton X-114 phase par-
181 titioning experiments revealed that Rv1813c is not an integral membrane protein, in agreement with
182 the absence of any predicted transmembrane domains (**Fig. 3D**) and its exclusion from the *Mtb* cell

183 wall **(Supplementary Fig. S1)**. Consistently, Rv1813c was extracted from mitochondrial mem-
184 branes by sodium carbonate treatment, a characteristic feature of peripheral membrane proteins
185 (**Fig. 3E**). Since Rv1813c was not released from mitochondria by high salt washes (**Fig. 3F**) and was
186 protected from proteinase K digestion of intact mitochondria (**Fig. 3G**), we concluded that Rv1813c
187 resides inside mitochondria. In addition, Rv1813c was partially released from mitochondria upon
188 the specific rupture of mitochondrial outer membranes in hypotonic buffer indicating that Rv1813c
189 accumulates into the mitochondrial IMS where it could be weakly attached to the internal or external
190 sides of mitochondrial outer or inner membranes respectively (**Fig. 3H**).
191
192 **Rv1813c and orthologous proteins are addressed to mitochondria in mammalian cells**
193 We next extended the analysis to mammalian cells. Native and myc-tagged Rv1813c were transi-
194 ently expressed in HeLa cells and their intracellular localization was determined by confocal mi-
195 croscopy. As observed in *Dictyostelium*, Rv1813c was efficiently targeted to mitochondria in HeLa
196 cells (**Fig. 4A and Supplementary Fig. S4**) without any detectable effects on the mitochondrial
197 morphology (**Fig. 4B**). MMA_1436 and MMA_2533, two *Mmar* orthologues of Rv1813c also local-
198 ized to mitochondria. However, in contrast to *Dictyostelium* cells, Rv1269c remained in the cytosol
199 similarly to MMA_4153, the *Mmar* orthologs of Rv1269c, which also showed a faint mitochondrial
200 localization (**Supplementary Fig. S4**). Although it might denote an intrinsic feature, we cannot rule
201 out that the folding of these proteins might not proceed appropriately in mammalian cells impeding
202 their efficient mitochondrial localization.
203 Whereas the overall morphology of mitochondria was preserved upon Rv1813c ectopic expression,
204 transmission electronic microscopy (TEM) revealed some ultrastructural modifications. Hence,
205 Rv1813c expressed in HeLa cells contained mitochondria with either normal or electron-dense ma-
206 trix, and the intra-cristae space appeared significantly enlarged compared to parental HeLa cells
207 **(Fig. 4C, 4D).** This altered mitochondrial morphology is reminiscent to what is observed in *Mtb*
208 infected macrophages (Abarca-Rojano et al., 2003). Since cristae membranes are enriched in resi-
209 dent proteins involved in oxidative phosphorylation, this particular ultrastructure might lead to sev-
210 eral mitochondrial energetic/metabolism consequences.
211
212 **Rv1813c overexpression enhances cell metabolism and mitochondrial ROS production**
213 Next, we investigated whether changes in the mitochondrial morphology might cause energy me-
214 tabolism disorders. Oxidative phosphorylation (OXPHOS) and glycolysis were simultaneously ana-
215 lyzed in intact cells making use of an extracellular flux analyzer (XF, Agilent Seahorse). In this assay,
216 mitochondrial respiratory characteristics are evaluated by recording oxygen consumption rate
217 (OCR) upon sequential chemical perturbation of selected mitochondrial functions (as detailed in
218 Fig. 5 legend). In Rv1813c transfected HeLa cells, basal respiration, ATP-linked respiration, maxi-
219 mal respiratory capacity and reserve capacity were significantly increased compared to parental

220 HeLa cells (**Fig. 5A-B**). Glycolysis was also assayed using a glycolysis stress test (Agilent Technol-
221 ogies) and measurements of extracellular acidification rates (ECAR) in incubation media. This assay
222 revealed similar glycolytic profiles in control and Rv1813c expressing HeLa cells (**Fig. 5C-D**). Next,
223 mitochondrial membrane potential was tested using flow cytometry of JC-1 stained cells. This as-
224 say revealed that expression of Rv1813c in Hela cells had no effect on $\Delta\Psi_M$ in resting cells (**Fig.**
225 **5E**). However, these cells showed a slight but significant increased mitochondrial ROS production
226 (**Fig. 5F**). Taken together, these results indicate that Rv1813c expression improves mitochondrial
227 respiratory capacities without altering glycolytic functions, driving cells into an energy activated
228 state. This higher mitochondrial respiration is associated with a moderate increased mitochondrial
229 free radical formation without changes in the mitochondrial membrane potential.
230
231 **Oxidative stress-induced translocation of cytochrome c is delayed in Rv1813c expressing**
232 **cells.**
233 We next assessed whether these mitochondrial alterations might alter the ability of Rv1813c ex-
234 pressing HeLa cells to cope with oxidative stress, a situation encountered during by *Mtb* infection.
235 We choose to monitor the release of Cytochrome c (Cyt-c) from mitochondria into the cytosol in
236 response to hydrogen peroxide, an early event in apoptotic cell death (Stridh et al., 1998). Hence,
237 cells were incubated with hydrogen peroxide for three hours, and the localization of Cyt-c and
238 Rv1813c was analyzed by confocal microscopy. As expected, Cyt-c showed a diffuse cytosolic
239 staining in 21% of parental HeLa cells upon addition of 0.1mM hydrogen peroxide (**Fig. 6A, 6B**).
240 Rv1813c release from mitochondria was also observed in cells overexpressing Rv1813c in re-
241 sponse to hydrogen peroxide treatments (Fig. **6A, 6C**). In contrast, Cyt-c release from mitochondria
242 into the cytosol was reduced in Rv1813c expressing cells, with only 7.9% of cells displaying a
243 cytosolic Cyt-c staining upon oxidative stress conditions (**Fig. 6A, B**). Note that cells with cytosolic
244 Cyt-c always showed a strict concomitant Rv1813c cytosolic localization, thus we did not detect
245 any cells harboring cytosolic Cyt-c and mitochondrial Rv1813c localizations together. Strikingly,
246 Rv1813c release from mitochondria was more frequently observed than Cyt-c translocation leading
247 to another cell population with Rv1813c in the cytosol but Cyt-c still in mitochondria (**Fig. 6D**). We
248 conclude that the massive exit of Rv1813c from mitochondria in response to oxidative stress might
249 delay the normal stress-induced Cyt-c translocation.
250
251 **Discussion**
252 Several intracellular pathogens (i.e. *Rickettsia*, *Legionella*, *Salmonella*) disrupt mitochondrial func-
253 tions during infection mainly due to indirect effects (Spier et al., 2019)(Garaude, 2019) but more
254 rarely by direct mitochondrial targeting of bacterial effectors having adverse functions (Hicks and
255 Galán, 2013). For instance, the EspF effector from enteropathogenic *E. coli* is addressed to mito-
256 chondria via a mitochondrial import signal and promotes caspase-mediated apoptosis in intestinal

257 epithelial cells (Hua et al., 2018). Furthermore, the MitF protein from *L. pneumophilia* was reported
258 to alter mitochondria fission dynamics and promote a Warburg-like phenotype in macrophages
259 (Escoll et al., 2017). Using bioinformatics screening and culture filtrate analysis, we have identified
260 Rv1813c from *Mtb* as a secreted protein. The protein serves a role of vaccine adjuvant (Bertholet
261 et al., 2008) and is highly immunogenic (Liang et al., 2019). The corresponding gene is non-essential
262 for *Mtb* growth, however its deletion impairs *Mtb* virulence in a low dose murine model (Bretl et al.,
263 2012). To our knowledge, no functional studies have been reported so far, thus the molecular basis
264 of this attenuation is still unknown. Interestingly, Rv1813c expression is regulated by MprA and
265 DosR proteins (Bretl et al., 2012). DosR is a transcriptional regulator induced by host intracellular
266 stimuli, such as nitric oxide (NO), carbon monoxide (CO), and hypoxia (Bretl et al., 2012), while
267 MrpA responds to environmental stress and residence within the macrophage (Haydel and Clark-
268 Curtiss, 2004) (Pan et al., 2020) and is required during infection (Zahrt and Deretic, 2001). Accord-
269 ingly, reference transcriptomes have revealed that Rv1813c is over-expressed (x2 and x4, 24h and
270 48h post-infection, respectively) in activated infected macrophages (Schnappinger et al., 2006),
271 and in the BALB/c mouse model (x4, x5 then x6 respectively after 7, 14 and 21 days post-infection)
272 (Talaat et al., 2004).
273 In this study, we established that Rv1813c belongs to a new protein family constitutively secreted
274 by *Mtb* in culture medium and specifically addressed to mitochondria where it accumulates the IMS
275 when ectopically expressed in host cells (**Fig. S1 and Fig. 2-4**). We solved the structure of Rv1813c
276 that included a new protein fold with no similarity with any structures solved to date **(Fig. 1**). Inter-
277 estingly, this small 9 kDa conserved folded domain was sufficient to specifically address the protein
278 into mitochondria (**Fig. 2C**). Furthermore, we demonstrated that this localization subsequently en-
279 hances OXPHOS and inhibits cytochrome-c exit upon oxidative stress in Rv1813c-expressing cells.
280 These Rv1813c-dependent phenotypes might be connected to important host defense mecha-
281 nisms against *Mtb* infections and will have to be further addressed in *Mtb* infected cells.
282 Would the increased host cell mitochondrial ATP production induced by a *Mtb* effector protein bring
283 any benefits to the bacteria for its intracellular replication or for avoiding normal host defense mech-
284 anisms? The activation of macrophages in response to *Mtb* infection is known to induce their po-
285 larization toward the toward an M1 profile (Shi et al., 2019). This important step is achieved by a
286 metabolic reprogramming after NF-kB pathway activation either by pathogen-associated molecular
287 patterns (PAMPs) or IFNγ. NF-kB promotes the expression of the inducible nitric oxide synthase
288 (iNOS) and subsequent nitric oxide (NO) release. Besides bactericidal activity, NO directly inacti-
289 vates the electron transfer chain (ETC) proteins, triggering a complex series of events, mainly de-
290 pendent on the production of reactive oxygen species (ROS) and change in the metabolites balance
291 (*i.e.* NAD/NADP ratio). When the Krebs cycle is consequently blocked, citrate accumulates enhanc-
292 ing glycolysis and lipids biosynthesis. In addition, succinate also accumulates leading to HIF-1α
293 (Hypoxia-inducible factor-1) stabilization, which completes this metabolic switch similarly to the

294 Warburg effect observed in tumors (Shi et al., 2016). HIF-1α not only promotes the expression of
295 enzymes involved in glycolytic ATP production, but also induces expression pattern leading to syn-
296 thesis of important immune effectors, including inflammatory cytokines and chemokines under
297 normoxic conditions (Wilson et al., 2019).
298 Very few studies have assessed the precise metabolic state of *Mtb* infected cells (Mohareer et al.,
299 2020) and they have led to contradictory results. Recently, bioenergetic analyzes have been per-
300 formed in infected macrophages. Hence, XF experiments and metabolites analysis have revealed
301 a decrease of cell energetic flux through glycolysis and the TCA cycle in infected macrophages.
302 Consequently, the total level of ATP produced in *Mtb* infected cells 5 and 24 hours post infection
303 is reduced (Cumming et al., 2018). This observations confirm previous results indicating that the
304 glycolytic flux was reduced in macrophages infected with virulent H37rv bacteria, a possible hall-
305 mark of a bacterial effector-induced incomplete or delayed metabolic shift (Simeone et al., 2012).
306 On the contrary, other studies have suggested that maintaining host cell ATP production is benefi-
307 cial for *Mtb* in order to avoid ROS production and apoptosis. For instance, a much higher ATP/ADP
308 ration was observed in H37Rv-infected cells compared to cells infected with avirulent H37Ra
309 (Jamwal et al., 2013)(Jamwal et al., 2016). In agreement, an elevated ATP/ADP ratio was also cor-
310 related to lower apoptosis rates observed in H37Rv-infected cells (Jamwal et al., 2013)(Mehrotra et
311 al., 2014). Taken together, these data indicate that maintaining a high ATP production might be
312 beneficial to delay a deleterious full metabolic shift and/or apoptosis of the host cell. Consistent
313 with this hypothesis, secretion of Rv1813c could participate in maintaining a higher ATP production
314 within mitochondria during *Mtb* infection.
315 Mitochondrial proton leak generated from the ETC is the major source of mitochondrial ROS. Ex-
316 cessive ROS amounts result in multiple effects including cytochrome-c translocation followed by
317 caspase dependent apoptosis as well as inflammasome activation (Jamwal et al., 2013). Accord-
318 ingly, the slight increase of ROS observed in resting Rv1813c-expressing cells (**Fig. 5F**) might be
319 due ETC and/or ATP synthase boosted functions raising the ATP production in these cells. Inter-
320 estingly, the artificial increase of ROS by exogenous hydrogen peroxide did not readily induce the
321 release of Cyt-c from mitochondria in Rv1813c-expressing cells compared to parental HeLa cells.
322 The release of Cytochrome c from mitochondria is an early event in apoptotic cell death and an
323 early defense mechanism in infected *Mtb* macrophages (Li et al., 1997). Thus, this Rv1813c-based
324 inhibition of this process might bring some advantages for *Mtb*. The molecular mechanism respon-
325 sible for this inhibition will be further addressed.
326 In summary, this study provides some detailed suggestions for the possible regulatory functions of
327 Rv1813c in the metabolic and apoptotic responses happening in *Mtb* infected macrophages.
328
329
330

Detailed methods are provided in Supplementary Materials and Methods of this paper and include the following:

- Purification of recombinant ^{6}His-Rv1813c$_{28-143}$ in *E. coli*
- Solution structure of Rv1813c$_{28-143}$
- Antibodies
- Preparation of *Mycobacterium tuberculosis* culture
- Mycobacterial cell fractionation
- Protein Electrophoresis and Western Blot
- Cell culture and transfection conditions
- Mitochondria isolation and biochemical treatments
- Immunocytochemistry
- Flow cytometry analysis of JC-1, MitoSox and Annexin 5/PI stained cells
- MACS enrichment of CD4-Rv1813c transfected cells
- Extracellular flux analysis
- Transmission electron microscopy

AUTHOR CONTRIBUTION

MM, AdV, PB, YMB, OP, TA, LH, JG, CG, GM, FL and MCG performed experiments; MM, GM, CG, ON, FL and MCG analyzed the data; FL and MCG conceived this study; All authors contributed to manuscript writing.

AKNOWLEDGEMENTS

Flow cytometry and microscopy analyzes of uninfected cells were performed at the Montpellier RIO imaging facility of the University of Montpellier, member of the national infrastructure France-BioImaging, supported by the French National Research Agency (ANR-10-INBS-04, “Investments for the future”). The CBS acknowledges support from the French Infrastructure for Integrated Structural Biology (FRISBI) ANR-10-INSB-05-01. The following reagents were obtained through BEI Resources, NIAID, NIH: Monoclonal Anti-*M. tuberculosis* GlnA (Gene Rv2220), Clone IT-58 (CBA5) (produced *in vitro*), NR-44103; Polyclonal Anti-*Mycobacterium tuberculosis* FtsZ (Gene Rv2150c) (antiserum rabbit).

DECLATION OF INTERESTS

366 The authors declare no competing interests.
367
368 **References**
369 Abarca-Rojano, E., Rosas-Medina, P., Zamudio-Cortéz, P., Mondragón-Flores, R., and Sánchez-
370 García, F.J. (2003). Mycobacterium tuberculosis virulence correlates with mitochondrial cyto-
371 chrome c release in infected macrophages. Scand J Immunol *58*, 419–427.
372 https://doi.org/10.1046/j.1365-3083.2003.01318.x.
373
374 Albrethsen, J., Agner, J., Piersma, S.R., Højrup, P., Pham, T.V., Weldingh, K., Jimenez, C.R., An-
375 dersen, P., and Rosenkrands, I. (2013). Proteomic profiling of Mycobacterium tuberculosis identi-
376 fies nutrient-starvation-responsive toxin-antitoxin systems. Mol Cell Proteomics *12*, 1180–1191.
377 https://doi.org/10.1074/mcp.M112.018846.
378
379 Bertholet, S., Ireton, G.C., Kahn, M., Guderian, J., Mohamath, R., Stride, N., Laughlin, E.M., Bald-
380 win, S.L., Vedvick, T.S., Coler, R.N., et al. (2008). Identification of Human T Cell Antigens for the
381 Development of Vaccines Against Mycobacterium Tuberculosis. J Immunol *181*, 7948–7957. .
382
383 Bretl, D.J., He, H., Demetriadou, C., White, M.J., Penoske, R.M., Salzman, N.H., and Zahrt, T.C.
384 (2012). MprA and DosR coregulate a Mycobacterium tuberculosis virulence operon encoding
385 Rv1813c and Rv1812c. Infect. Immun. *80*, 3018–3033. https://doi.org/10.1128/IAI.00520-12.
386
387 Cardenal-Muñoz, E., Barisch, C., Lefrançois, L.H., López-Jiménez, A.T., and Soldati, T. (2017).
388 When Dicty Met Myco, a (Not So) Romantic Story about One Amoeba and Its Intracellular Patho-
389 gen. Front Cell Infect Microbiol *7*, 529. https://doi.org/10.3389/fcimb.2017.00529.
390
391 Cumming, B.M., Addicott, K.W., Adamson, J.H., and Steyn, A.J. (2018). Mycobacterium tuberculo-
392 sis induces decelerated bioenergetic metabolism in human macrophages. Elife *7*.
393 https://doi.org/10.7554/eLife.39169.
394
395 Daleke, M.H., Ummels, R., Bawono, P., Heringa, J., Vandenbroucke-Grauls, C.M.J.E., Luirink, J.,
396 and Bitter, W. (2012). General secretion signal for the mycobacterial type VII secretion pathway.
397 Proc Natl Acad Sci U S A *109*, 11342–11347. https://doi.org/10.1073/pnas.1119453109.
398
399 Davidson, A.J., King, J.S., and Insall, R.H. (2013). The use of streptavidin conjugates as immunob-
400 lot loading controls and mitochondrial markers for use with Dictyostelium discoideum. BioTech-
401 niques *55*, 39–41. https://doi.org/10.2144/000114054.
402

Escoll, P., Song, O.-R., Viana, F., Steiner, B., Lagache, T., Olivo-Marin, J.-C., Impens, F., Brodin, P., Hilbi, H., and Buchrieser, C. (2017). Legionella pneumophila Modulates Mitochondrial Dynamics to Trigger Metabolic Repurposing of Infected Macrophages. Cell Host Microbe *22*, 302-316.e7. https://doi.org/10.1016/j.chom.2017.07.020.

Feltcher, M.E., Sullivan, J.T., and Braunstein, M. (2010). Protein export systems of Mycobacterium tuberculosis: novel targets for drug development? Future Microbiol *5*, 1581–1597. https://doi.org/10.2217/fmb.10.112.

Fujiki, Y., Hubbard, A.L., Fowler, S., and Lazarow, P.B. (1982). Isolation of intracellular membranes by means of sodium carbonate treatment: application to endoplasmic reticulum. J Cell Biol *93*, 97–102. https://doi.org/10.1083/jcb.93.1.97.

Garaude, J. (2019). Reprogramming of mitochondrial metabolism by innate immunity. Curr Opin Immunol *56*, 17–23. https://doi.org/10.1016/j.coi.2018.09.010.

Gracy, J., and Chiche, L. (2005). PAT: a protein analysis toolkit for integrated biocomputing on the web. Nucleic Acids Res *33*, W65-71. https://doi.org/10.1093/nar/gki455.

Haydel, S.E., and Clark-Curtiss, J.E. (2004). Global expression analysis of two-component system regulator genes during Mycobacterium tuberculosis growth in human macrophages. FEMS Microbiol. Lett. *236*, 341–347. https://doi.org/10.1016/j.femsle.2004.06.010.

Hicks, S.W., and Galán, J.E. (2013). Exploitation of eukaryotic subcellular targeting mechanisms by bacterial effectors. Nat Rev Microbiol *11*, 316–326. https://doi.org/10.1038/nrmicro3009.

Hmama, Z., Peña-Díaz, S., Joseph, S., and Av-Gay, Y. (2015). Immunoevasion and immunosuppression of the macrophage by Mycobacterium tuberculosis. Immunological Reviews *264*, 220–232. https://doi.org/10.1111/imr.12268.

Holm, L., and Rosenström, P. (2010). Dali server: conservation mapping in 3D. Nucleic Acids Res *38*, W545-549. https://doi.org/10.1093/nar/gkq366.

Hua, Y., Yan, K., and Wan, C. (2018). Clever Cooperation: Interactions Between EspF and Host Proteins. Front. Microbiol. *9*. https://doi.org/10.3389/fmicb.2018.02831.

439 Jamwal, S., Midha, M.K., Verma, H.N., Basu, A., Rao, K.V.S., and Manivel, V. (2013). Characterizing virulence-specific perturbations in the mitochondrial function of macrophages infected with Mycobacterium tuberculosis. Sci Rep *3*, 1328. https://doi.org/10.1038/srep01328.

443 Jamwal, S.V., Mehrotra, P., Singh, A., Siddiqui, Z., Basu, A., and Rao, K.V.S. (2016). Mycobacterial escape from macrophage phagosomes to the cytoplasm represents an alternate adaptation mechanism. Scientific Reports *6*, 23089. https://doi.org/10.1038/srep23089.

447 Kostakioti, M., Newman, C.L., Thanassi, D.G., and Stathopoulos, C. (2005). Mechanisms of Protein Export across the Bacterial Outer Membrane. J Bacteriol *187*, 4306–4314. https://doi.org/10.1128/JB.187.13.4306-4314.2005.

451 Lee, J.-M., Cho, H.Y., Cho, H.J., Ko, I.-J., Park, S.W., Baik, H.-S., Oh, J.-H., Eom, C.-Y., Kim, Y.M., Kang, B.S., et al. (2008). O2- and NO-sensing mechanism through the DevSR two-component system in Mycobacterium smegmatis. J. Bacteriol. *190*, 6795–6804. https://doi.org/10.1128/JB.00401-08.

456 Li, P., Nijhawan, D., Budihardjo, I., Srinivasula, S.M., Ahmad, M., Alnemri, E.S., and Wang, X. (1997). Cytochrome c and dATP-dependent formation of Apaf-1/caspase-9 complex initiates an apoptotic protease cascade. Cell *91*, 479–489. https://doi.org/10.1016/s0092-8674(00)80434-1.

460 Liang, Y., Zhang, X., Bai, X., Yang, Y., Gong, W., Wang, T., Ling, Y., Zhang, J., Wang, L., Wang, J., et al. (2019). Immunogenicity and Therapeutic Effects of Latency-Associated Genes in a Mycobacterium Tuberculosis Reactivation Mouse Model. Hum Gene Ther Methods *30*, 60–69. https://doi.org/10.1089/hgtb.2018.211.

465 Målen, H., Berven, F.S., Fladmark, K.E., and Wiker, H.G. (2007). Comprehensive analysis of exported proteins from Mycobacterium tuberculosis H37Rv. Proteomics *7*, 1702–1718. https://doi.org/10.1002/pmic.200600853.

469 McGuffin, L.J., Bryson, K., and Jones, D.T. (2000). The PSIPRED protein structure prediction server. Bioinformatics *16*, 404–405. https://doi.org/10.1093/bioinformatics/16.4.404.

471 Mehrotra, P., Jamwal, S.V., Saquib, N., Sinha, N., Siddiqui, Z., Manivel, V., Chatterjee, S., and Rao, K.V.S. (2014). Pathogenicity of Mycobacterium tuberculosis is expressed by regulating metabolic thresholds of the host macrophage. PLoS Pathog. *10*, e1004265. https://doi.org/10.1371/journal.ppat.1004265.

Mohareer, K., Medikonda, J., Vadankula, G.R., and Banerjee, S. (2020). Mycobacterial Control of Host Mitochondria: Bioenergetic and Metabolic Changes Shaping Cell Fate and Infection Outcome. Front. Cell. Infect. Microbiol. *10*. https://doi.org/10.3389/fcimb.2020.00457.

Müller-Taubenberger, A., Kortholt, A., and Eichinger, L. (2013). Simple system--substantial share: the use of Dictyostelium in cell biology and molecular medicine. Eur J Cell Biol *92*, 45–53. https://doi.org/10.1016/j.ejcb.2012.10.003.

Nicholson, K.R., Mousseau, C.B., Champion, M.M., and Champion, P.A. (2021). The genetic proteome: Using genetics to inform the proteome of mycobacterial pathogens. PLOS Pathogens *17*, e1009124. https://doi.org/10.1371/journal.ppat.1009124.

Pan, F., Ye, T., Sun, P., Gui, S., Liang, B., Li, L., Zheng, D., Wang, J., Hesketh, R.L., Yang, L., et al. (2020). Time Course of Lung Changes On Chest CT During Recovery From 2019 Novel Coronavirus (COVID-19) Pneumonia. Radiology 200370–200370. https://doi.org/10.1148/radiol.2020200370.

Penn, B.H., Netter, Z., Johnson, J.R., Von Dollen, J., Jang, G.M., Johnson, T., Ohol, Y.M., Maher, C., Bell, S.L., Geiger, K., et al. (2018). An Mtb-Human Protein-Protein Interaction Map Identifies a Switch between Host Antiviral and Antibacterial Responses. Mol Cell *71*, 637-648.e5. https://doi.org/10.1016/j.molcel.2018.07.010.

Perkowski, E.F., Zulauf, K.E., Weerakoon, D., Hayden, J.D., Ioerger, T.R., Oreper, D., Gomez, S.M., Sacchettini, J.C., and Braunstein, M. (2017). The EXIT Strategy: an Approach for Identifying Bacterial Proteins Exported during Host Infection. MBio *8*. https://doi.org/10.1128/mBio.00333-17.

Schnappinger, D., Schoolnik, G.K., and Ehrt, S. (2006). Expression profiling of host pathogen interactions: how Mycobacterium tuberculosis and the macrophage adapt to one another. Microbes Infect *8*, 1132–1140. https://doi.org/10.1016/j.micinf.2005.10.027.

Shi, L., Eugenin, E.A., and Subbian, S. (2016). Immunometabolism in Tuberculo
sis. Front Immunol *7*, 150. https://doi.org/10.3389/fimmu.2016.00150.

Shi, L., Jiang, Q., Bushkin, Y., Subbian, S., and Tyagi, S. (2019). Biphasic Dynamics of Macrophage Immunometabolism during Mycobacterium tuberculosis Infection. MBio *10*. https://doi.org/10.1128/mBio.02550-18.

Simeone, R., Bobard, A., Lippmann, J., Bitter, W., Majlessi, L., Brosch, R., and Enninga, J. (2012).

513 Phagosomal rupture by Mycobacterium tuberculosis results in toxicity and host cell death. PLoS
514 Pathog *8*, e1002507. https://doi.org/10.1371/journal.ppat.1002507.
515
516 de Souza, G.A., Leversen, N.A., Målen, H., and Wiker, H.G. (2011). Bacterial proteins with cleaved
517 or uncleaved signal peptides of the general secretory pathway. J Proteomics *75*, 502–510.
518 https://doi.org/10.1016/j.jprot.2011.08.016.
519
520 Spier, A., Stavru, F., and Cossart, P. (2019). Interaction between Intracellular Bacterial Pathogens
521 and Host Cell Mitochondria. Bacteria and Intracellularity 3–13. https://doi.org/10.1128/microbi-
522 olspec.BAI-0016-2019.
523
524 Steinert, M. (2011). Pathogen-host interactions in Dictyostelium, Legionella, Mycobacterium and
525 other pathogens. Semin Cell Dev Biol *22*, 70–76. https://doi.org/10.1016/j.semcdb.2010.11.003.
526
527 Stridh, H., Kimland, M., Jones, D.P., Orrenius, S., and Hampton, M.B. (1998). Cytochrome c re-
528 lease and caspase activation in hydrogen peroxide- and tributyltin-induced apoptosis. FEBS Lett
529 *429*, 351–355. https://doi.org/10.1016/s0014-5793(98)00630-9.
530
531 Talaat, A.M., Lyons, R., Howard, S.T., and Johnston, S.A. (2004). The temporal expression profile
532 of Mycobacterium tuberculosis infection in mice. Proc. Natl. Acad. Sci. U.S.A. *101*, 4602–4607.
533 https://doi.org/10.1073/pnas.0306023101.
534
535 Troll, H., Malchow, D., Müller-Taubenberger, A., Humbel, B., Lottspeich, F., Ecke, M., Gerisch, G.,
536 Schmid, A., and Benz, R. (1992). Purification, functional characterization, and cDNA sequencing of
537 mitochondrial porin from Dictyostelium discoideum. J Biol Chem *267*, 21072–21079. .
538
539 Tucci, P., Portela, M., Chetto, C.R., González-Sapienza, G., and Marín, M. (2020). Integrative pro-
540 teomic and glycoproteomic profiling of Mycobacterium tuberculosis culture filtrate. PLoS One *15*,
541 e0221837. https://doi.org/10.1371/journal.pone.0221837.
542
543 Turapov, O., Waddell, S.J., Burke, B., Glenn, S., Sarybaeva, A.A., Tudo, G., Labesse, G., Young,
544 D.I., Young, M., Andrew, P.W., et al. (2014). Oleoyl coenzyme A regulates interaction of transcrip-
545 tional regulator RaaS (Rv1219c) with DNA in mycobacteria. J Biol Chem *289*, 25241–25249.
546 https://doi.org/10.1074/jbc.M114.577338.
547
548 Wilson, J.L., Mayr, H.K., and Weichhart, T. (2019). Metabolic Programming of Macrophages: Impli-
549 cations in the Pathogenesis of Granulomatous Disease. Front Immunol *10*, 2265.

550 https://doi.org/10.3389/fimmu.2019.02265.
551
552 Winden, V.J.C. van, Houben, E.N.G., and Braunstein, M. (2019). Protein Export into and across
553 the Atypical Diderm Cell Envelope of Mycobacteria. Microbiology Spectrum *7*.
554 https://doi.org/10.1128/microbiolspec.GPP3-0043-2018.
555
556 Ye, Y., and Godzik, A. (2004). Database searching by flexible protein structure alignment. Protein
557 Sci *13*, 1841–1850. https://doi.org/10.1110/ps.03602304.
558
559 Zahrt, T.C., and Deretic, V. (2001). Mycobacterium tuberculosis signal transduction system re-
560 quired for persistent infections. PNAS *98*, 12706–12711. https://doi.org/10.1073/pnas.221272198.
561

562 **FIGURE LEGENDS**

563

564 **Fig. 1: Rv1813c defines a new protein family.**
565 **(A)** *M. tuberculosis* and *M. marinum* Rv1813c homologues sequence alignments. The secondary
566 structure of Rv1813c is reported above the alignment. The yellow numbers indicate the cysteine
567 engaged in disulfide bridges. **(B)** Rv1813c structure determined by multi-dimensional NMR. Three
568 cartoon representations of the structure. Only four residues of the N-terminal unfolded part of the
569 protein (residues 28-57) are represented. The cysteine residues, all engaged in disulfide bridges are
570 represented in yellow while the two solvent-exposed tryptophan amino acids are represented in
571 orange.
572

573 **Fig. 2: Mitochondrial localization of Rv1813c in *Dictyostelium.***
574 *Dictyostelium* cells expressing the indicated constructs were fixed, processed for immunofluores-
575 cence, and analyzed by confocal microscopy (Airyscan). **(A)** Colocalization of myc-Rv1813c (de-
576 tected with a rabbit polyclonal to Rv1813c) and mitochondrial Mitoporin in ring shaped structures.
577 **(B)** Labeling of mitochondria of the indicated cells lines with Mitotracker deep red dye. Close-ups
578 of mitochondria are shown in the inserts. **(C)** Maximum fluorescence intensity projection of Z con-
579 focal sections of cells expressing the full-length protein (myc-Rv1813c), the sole structured domain
580 (myc-Rv1813c_49-143) and the unfolded domain (myc-Rv1813c_28-56) labeled with an anti-myc
581 antibody. Cell contours are indicated by dotted lines. Bar, 5 µm.
582

583 **Fig. 3: Biochemical analysis of Rv1813c mitochondrial localization in *Dictyostelium.***

584 **(A)** Schematic ultrastructure of a single crista in mitochondria. Abbreviations: IMS, intermembrane
585 space; IM, inner membrane; OM, outer membrane. (**B)** Fractionation scheme of differential centrif-
586 ugation steps used to purify the Rv1813c enriched fraction from *Dictyostelium* cells. P and S rep-
587 resent pellet and supernatant, respectively **(C)** Fractions were analyzed by immunoblotting with
588 antibodies to Mitoporin (mitochondria), EHD (endocytic vacuoles) and myc-tag (myc-Rv1813c). **(D)**
589 The mitochondrial fraction was fractionated by Triton X114 extraction. The separated Triton X-114
590 (TX) and aqueous (W) phases were analyzed as above. Rv1813c is not extracted by Triton X-114
591 indicating no insertion inside membranes. **(E)** Mitochondria were incubated in sodium carbonate
592 for 30 min. Rv1813c is mainly detected in the supernatant fraction (S) after centrifugation at 100,000
593 g of treated mitochondria, a characteristic of soluble and/or membrane peripheral proteins. **(F)** For
594 high-salt protein extraction, mitochondria were incubated in buffer ± 200 mM KCl for 30 min and
595 centrifuged at 16,000 g for 10 min. **(G)** Intact or Triton X100 treated mitochondria were subjected
596 to proteinase K digestion for 30 min and analyzed by immunoblotting. **(H)** Mitochondria swelling
597 was induced by hypotonic buffer incubation for 30 min. Released proteins (S1) from broken outer
598 membranes (P1) were recovered by centrifugation at 16,000g for 10 min and analyzed by western
599 blotting to detect myc-Rv1813c, Mitoporin (mitochondrial outer membrane) and mitochondrial 3-
600 methylcrotonyl-CoA carboxylase α (MCCC1; mitochondrial matrix). Non-treated (NT) mitochondria
601 incubated for 30 min in mitochondria isolation buffer A served as release specificity control.
602
603 **Fig. 4: Targeting of Rv1813c to mitochondria in mammalian cells**
604 **(A)** Confocal microscopy analysis of HeLa cells transiently expressing myc-Rv1813. Cells were
605 fixed 48h post-transfection, processed for immunofluorescence with antibodies to RV1813c and
606 cytochrome c, and analyzed by Airyscan microscopy. Bar, 10 µm. **(B)** Quantitative analysis of the
607 mitochondria morphology observed in HeLa cells transiently transfected with pCI-myc-Rv1813 or
608 empty vector as control. Mitochondria morphology was manually identified by confocal microscopy
609 and classified in one hundred cells of one representative experiment from three independent ana-
610 lyzes. **(C, D)** Representative mitochondria ultrastructure determined by transmission electronic mi-
611 croscopy of MACS enriched HeLa cells transiently transfected with pMACS-4-IRES-II Rv1813c (C)
612 or vector alone (D). Black arrows indicate some enlarged intra-cristae spaces in Rv1813c express-
613 ing cells. Bars, 500 nm. **(E)** Box-plot of intra-cristae spaces measurements for the indicated cell
614 lines (100 random measurements each, **** $p<0.0001$ in student test). The bar inside the box indi-
615 cates the median value. The bottom and top edges of the box indicate the 25th and 75th percen-
616 tiles, respectively. The whiskers extend to the most extreme data points not considered outliers.
617
618 **Fig. 5: Functional consequences of Rv1813c mitochondrial localization**

619 **(A,B)** Analysis of cell respiratory functions. HeLa cells were transiently transfected with pMACS-4-
620 IRES-II Rv1813c or vector alone and enriched to >94% of expressing cells. Cell respiratory profiles
621 (OCR) (A) and respiratory parameters (B) were obtained using an extracellular flux analyzer (Sea-
622 horse XF analyzer) and the mitochondrial respiration test. After reaching basal respiration, cells
623 were subjected to 1 µM oligomycin to inhibit the ATP synthase and measure the mitochondrial ATP-
624 linked OCR, followed by 1µM FCCP (cyanide-4-[trifluoromethoxy]phenylhydrazone) to uncouple
625 mitochondrial respiration and maximize OCR, and finally 1 µM antimycin A (AntiA) and 100 nM
626 rotenone (Rot) to inhibit complex III and I in the ETC respectively, and shut down respiration. In (B),
627 analyzed respiratory parameters are non-mitochondrial respiration (Non-Mito Resp), basal respira-
628 tion (Basal Resp), maximal respiration (Max Resp), proton leak, ATP production (ATP Prod) and
629 spare respiratory capacity (Spare Resp Cap). **(C,D)** Analysis of glycolytic functions. Extracellular
630 acidification (ECAR) profiles (C) and glycolytic parameters (D) of the same MACS enriched trans-
631 fected cells were determined simultaneously to OCR analysis using the glycolysis stress test and
632 the XF analyzer. After reaching non-glycolytic acidification, 10 mM glucose was added, followed by
633 1 µM oligomycin (Oligo) to inhibit the ATP synthase and induce maximal glycolysis. Finally, 100 mM
634 2-deoxyglucose (2-DG) was added to shut down glycolysis. This last injection resulted in a de-
635 creased ECAR confirming that the recorded ECAR was only due to glycolysis. In D, analyzed gly-
636 colitic parameters are non-glycolitic acidification (Non-Gly Acid), glycolytic capacity (Gly Capacity),
637 glycolysis (Gly) and glycolytic reserve (Gly Reserve). Values are means ± sd. Student's t test relative
638 to HeLa cells #, $p < 0.000001$, ** $p < 0.0005$, * $p < 0.005$, ns non-significant. In **(E)** and **(F)**, HeLa
639 cells were transiently transfected with pCI-myc-Rv1813c or empty vector as control and analyzed
640 48h later by flow cytometry **(E)** Flow cytometry analysis of the indicated HeLa cell lines stained with
641 JC-1 to monitor mitochondrial membrane potential. JC-1 Red/Green ratio were calculated and ex-
642 pressed as the % of this ratio in HeLa cells. Values are means ± s.e.m. of three independent exper-
643 iments. ns, not significantly different Student's t-test. **(F)** Flow cytometry analysis of MitoSox
644 stained HeLa cell lines. MitoSox fluorescence was expressed as the % of fluorescence in HeLa
645 cells. Values are means ± s.e.m. of three independent experiments, ** $p \leq 0.01$ Student's t-test.

646

647 **Fig. 6: Analysis of Cyt-c and Rv1813c release from mitochondria upon oxidative stress**
648 **(A)** Confocal microscopy analysis of HeLa cells transiently expressing myc-Rv1813.
649 48h post-transfection, cells were treated with 0.1 or 0.2 mM hydrogen peroxide for three hours,
650 fixed, processed for immunofluorescence with anti-Cytochrome c (green) and anti-Rv1813c (red)
651 antibodies, and observed by confocal microscopy. Nuclei were stained with Hoechst (blue). White
652 arrows and white stars indicate cells with Cyt-c in mitochondria and cytosol respectively. Scale bar,
653 10 µm **(B, C, D)** Quantification of cells with Cyt-c in cytosol (B), with Rv1813c in cytosol (C) and
654 Rv1813c in cytosol but Cyt-c in mitochondria (D) upon incubation with hydrogen peroxide for three

655 hours. Values are means ± s.e.m. of three independent experiments, with 100 cells analyzed for
656 each condition, * $p<0.05$ Student's t-test.
657
658
659 **SUPPLEMENTARY DATA LEGENDS**
660 **Fig. S1: Rv1813 is detected in *M. tuberculosis* culture filtrate but not in cellular fractions**. Ly-
661 sate obtained from *M. tuberculosis* H37Rv strain grown in Sauton's medium to logarithmic phase
662 (OD_{580}~0.7) were fractionated and probed with anti-Rv1813 polyclonal antibodies. Culture filtrates
663 were obtained from the same culture. Anti-FtsZ (FtsZ is a cytoplasmic protein), anti-GlnA (GlnA is
664 a membrane protein) and anti-RpfB (RpfB is a membrane and cell-wall anchored protein) antibodies
665 were used to confirm the purity of mycobacterial fractions.
666
667 **Fig. S2: ^{1}H-^{15}N HSQC spectrum of Rv1813c**
668 This spectrum was obtained at 800 MHz, 20°C and pH 6,8 with 0.3 mM ^{15}N-uniformly labeled sam-
669 ple. Cross peak assignments are indicated using the one-letter amino acid code and number fol-
670 lowing the full-length protein sequence numbering.
671
672 **Fig. S3: Confocal microscopy analysis of Rv1813c family members localization in *Dictyoste-***
673 ***lium.***
674 *Dictyostelium* cells expressing the indicated constructs were fixed, processed for immunofluores-
675 cence, and analyzed by confocal microscopy (Airyscan).
676 **(A)** Cellular localization of Nt-GFP-tagged Rv1813c. **(B)** Mitochondrial localization of untagged
677 Rv1813c expressed in *Dictyostelium*. Rv1813c was labeled with a rabbit pAb anti-Rv1813c anti-
678 body. Rv1813c colocalizes with Mitoporin, a mitochondrial specific protein. **(C)** Mitoporin localiza-
679 tion in untransfected parental Ax2 cells. Cells were labeled with a mouse mAb to mitoporin revealing
680 characteristic ring shaped structures. A maximum projection of Z confocal sections is shown on
681 the right panel. **(D)** Localization of different Rv1813c family members of *M. tuberculosis* and *M.*
682 *marinum* expressed in *Dictyostelium and* revealed by anti-myc labelling. White arrows indicate so
683 mitochondria with affected shapes. Bar, 5 µm.
684
685 **Fig. S4: Rv1813c family localization in HeLa cells**
686 HeLa cells expressing the indicated constructs were fixed, processed for immunofluorescence, and
687 analyzed by confocal microscopy (Airyscan). Cells were colabeled either with rabbit polyclonal anti-
688 Rv1813c, mouse mAb anti-Cytochrome c, and mitotracker deep red (upper panel) or anti-myc,
689 rabbit anti-grp75 (mitochondria marker) and mitotracker deep red (lower panels). Bar, 10 µm.

690 **SUPPLEMENTARY TABLE 1**

691 **NMR and refinement statistics for RV1813 protein structures**

692

693

694 **NMR distance and dihedral constraints**

695 Distance constraints	
696 Total NOE	1516
697 Intra-residue	406
698 Inter-residue	
699 Sequential (|i – j| = 1)	465
700 Medium-range (|i – j| < 4)	253
701 Long-range (|i – j| > 5)	392
702 Hydrogen bonds	84
703 Total dihedral angle restraints	
704 ϕ	82
705 ψ	82

706

707 **Structure statistics**

708 Violations (mean and s.d.)	
709 Max. distance constraint violation (Å)	0.18 ± 0.03
710 Max. dihedral angle violation (º)	2.04 ± 0.48
711 Deviations from idealized geometry	
712 Bond lengths (Å)	0.0118 ± 0.0002
713 Bond angles (º)	1.2010 ± 0.0214
714 Impropers (º)	1.3446 ± 0.0861

715

716 **Ramachandran plot (%)**

717 Most favoured region	84.7
718 Additionally allowed region	14.2
719 Generously allowed region	0.8
720 Disallowed region	0.3

721

722 **Average pairwise r.m.s. deviation** (Å)**

723 Backbone	0.66 ± 0.18
724 Heavy	1.26 ± 0.19

725

726

727 ** "Pairwise r.m.s. deviation calculated among 20 refined structures for residues 31-116."

728 **Supplementary Materials and methods**

729

730 **Purification of recombinant ^{6}His-Rv1813c$_{28-143}$ in *E. coli***

731 *E. coli* BL21(DE3) strains containing pET::*rv1813*$_{28-143}$ vector were used to inoculate 1 L of LB medium
732 supplemented with ampicillin (100 µg/ml) and resulting cultures were incubated at 37 °C with shak-
733 ing until A_{600} reached ~0.5. Then, 1 mM final of isopropyl 1-thio-β-d-galactopyranoside was added
734 and growth was continued for 3 hr at 37 °C. The cells were harvested by centrifugation and the
735 resulting cell pellet was resuspended in buffer A (50 mM Tris-HCl pH 8.5, 150 mM NaCl, 2mM DTT).
736 Cells were then lysed by sonication and cell debris and insoluble materials were separated by cen-
737 trifugation. The pellet was then resuspended in buffer B (Buffer A + 8M Urea). After centrifugation
738 the supernatant was loaded into a Hitrap™ IMAC HP column (Amersham biosciences), equilibrated
739 in buffer B and 4 % of buffer C (buffer B supplemented with 300 mM of imidazole). The column was
740 washed with successive applications of buffer B (approximately 30 ml in total) to remove all the
741 impurities and then buffer C was increased over 20 ml to 100%. Fractions containing the Rv1813c
742 proteins were identified by SDS-PAGE, then pooled and concentrated using a 5 K cut-off concen-
743 trator to a 2mg/ml concentration. The protein was dialysed against buffer A over-night at 4°C. The
744 refolded protein was very unstable until removal of the 6His tag using 3C protease (4h digestion at
745 4°C). The protein was then loaded to a Superdex 75 26/60 (Amersham biosciences) size exclusion
746 column, equilibrated in buffer 20 mM Na-Phosphate pH 6.2, 150 mM NaCl. Again, fractions con-
747 taining the protein were identified by SDS-PAGE, then pooled and stored at -20°C until required.
748 This protocol was carried out for all the non-labelled constructs of Rv1813c as well as for ^{15}N and
749 ^{15}N -^{13}C labelled constructs, except that the cultures were grown in a minimum media containing
750 $^{15}NH_4Cl$ and $^{15}NH_4Cl/^{13}$C6-glucose as the sole nitrogen and carbon sources.

751

752 **Solution structure of Rv1813c (residue 28-143)**

753 All NMR experiments were generally carried out at 25°C on Bruker Avance III 700 (^{1}H-^{15}N double
754 resonance experiments) or Avance III 500 (^{1}H-^{13}C-^{15}N triple-resonance experiments) spectrometer
755 equipped with 5 mm z-gradient TCI cryoprobe, using the standard pulse sequences. NMR samples
756 consist of approximately 0.9 mM ^{15}N- or ^{15}N,^{13}C-labeled protein dissolved in 25 mM NaCitrate, 150
757 mM NaCl (pH 5.6) with 10% D_2O for the lock. ^{1}H chemical shifts were directly referenced to the
758 methyl resonance of DSS, while ^{13}C and ^{15}N chemical shifts were referenced indirectly to the absolute
759 ^{15}N/^{1}H or ^{13}C/^{1}H frequency ratios. All NMR spectra were processed and analyzed with GIFA. Back-
760 bone and Cβ resonance assignments were made using standard HNCA, HNCACB, CBCA(CO)NH,
761 HNCO, and HN(CA)CO experiments performed on the ^{15}N,^{13}C-labeled Rv1813c$_{28-143}$ sample. NOE
762 cross-peaks identified on 3D [^{1}H, ^{15}N] NOESY-HSQC (mixing time 120 ms) were assigned through
763 automated NMR structure calculations with CYANA 2.1, whereas NOE on 3D [^{1}H,^{13}C] NOESY-HSQC

764 were assigned manually. Backbone ϕ and ψ torsion angle constraints were obtained from a data-
765 base search procedure on the basis of backbone (^{15}N, H_N, $^{13}C'$, $^{13}C\alpha$, Hα, $^{13}C\beta$) chemical shifts using
766 the program TALOS+ (Shen et al., 2009). Hydrogen bond restraints were derived using standard
767 criteria on the basis of the amide ^{1}H / ^{2}H exchange experiments and NOE data. When identified, the
768 hydrogen bond was enforced using the following restraints: ranges of 1.8–2.0 Å for d(N-H,O), and
769 2.7–3.0 Å for d(N,O). The final list of restraints, from which values redundant with the covalent ge-
770 ometry has been eliminated. The 30 best structures (based on the final target penalty function val-
771 ues) were minimized with CNS 1.2 according the RECOORD procedure (Nederveen et al., 2005)
772 and analyzed with PROCHECK (Laskowski et al., 1993). The rmsds were calculated with MOLMOL
773 (Koradi et al., 1996). All statistics are given in Table 1. The chemical shift table was deposited in the
774 BMRB databank (accession number 7NHZ).
775
776 **Antibodies**
777 The following primary antibodies were used in this study: mouse anti-Myc (Invitrogen, #13-2500,
778 1:200 for immunofluorescence, 1:500 for immunoblot), mouse anti-cytochrome c (clone 6H2.B4,
779 BD PharMingen, 1:500 for immunofluorescence), mouse anti-*Dictyostelium* Mitoporin (70-100-1;
780 1:2000 for immunofluorescence and immunoblot) (Troll *et al.,* 1992), rabbit anti-Rv1813c raised
781 using recombinant Rv1813c (ProteoGenix SAS, Schiltigheim, France) (1:2000 for immunofluores-
782 cence, 1:5000 for immunoblot), rabbit anti-Grp75 (D13H4, XP #3593, Cell Signalling, 1:100 for im-
783 munofluorescence), rabbit anti-EHD (Dias *et al.,* 2012; 1:4000 for immunoblot). Secondary antibod-
784 ies used for immunoblotting were horseradish peroxidase (HRP)-conjugated donkey anti-mouse
785 IgG (H+L) (#715-035-151) and HRP-conjugated donkey anti-rabbit IgG (H+L) (#715-035-152) (Jack-
786 son ImmunoResearch). MCCC1 (mitochondrial matrix) was revealed by staining with HRP-conju-
787 gated streptavidin as previously described (Davidson et al., 2013). Secondary antibodies used for
788 immunofluorescence were Alexa-Fluor-568-conjugated goat anti-mouse IgG (H+L) (#A11031),
789 Alexa-Fluor-594-conjugated donkey anti-rabbit IgG (H+L) (#A21207), Alexa-Fluor-488-conjugated
790 goat anti-rabbit IgG (H+L) (#A11029) and Alexa-Fluor-488-conjugated donkey anti-rabbit IgG (H+L)
791 (#A21206) (ThermoFisher Scientific, Illkirsh, France). All secondary antibodies were used at 1:500
792 for immunofluorescence. Prolong Golf Antifade and Hoechst 33342 (#62249) were purchased from
793 Molecular Probes (ThermoFisher Scientific, Illkirsh, France).
794
795 **Preparation of *Mycobacterium tuberculosis* culture**
796 *M. tuberculosis* was grown in Middlebrook 7H9 liquid medium supplemented with 10% (v/v) Albu-
797 min-Dextrose Complex (ADC), 0.2% (v/v) glycerol and 0.1% Tween 80 (w/v), at 37°C in a roller in-
798 cubator. Bacterial growth was followed by measurement of absorbance at 580 nm, using a spec-
799 trophotometer, or by colony-forming unit (CFU) counting on 7H10 agar.
800

801 **Mycobacterial cell fractionation**

802 Mycobacteria cell fractionation was done as described else were (O.Turapov, Cell Report, 2018).
803 Briefly, cells were lysed in a buffer that contained 20 mM TrisHCl, pH 8.0, 150 mM NaCl, 20 mM
804 KCl, 10 mM MgCl2. Bacterial culture was homogenized with a Minilys homogenizer (Bertin Instru-
805 ments) using glass beads. A cocktail of proteinase/phosphatase inhibitors (Roche, UK) were used
806 in all buffers. Lysates were centrifuged for 1 hour at 27,000 x g, the pellets were washed in a car-
807 bonate buffer (pH 11) and used as a cell wall material. The supernatant was centrifuged again for 4
808 hours at 100,000 x g. The supernatants from this step was used as cytoplasmic fraction and the
809 pellets (membrane fractions) were washed once in carbonate buffer, pH 11 and twice in TBS buffer.
810 Proteins from cellular fractions were separated on SDS-PAGE. The purity of fractions was con-
811 firmed by the detection of diagnostic proteins as described below.

812

813 **Protein Electrophoresis and Western Blot**

814 Proteins were separated on 4%–20% gradient SERVA gels and transferred onto a nitrocellulose
815 membrane using a Trans-Blot® Turbo Transfer System (Bio-Rad) according to the manufacturer's
816 instruction. SignalFire Elite ECL Reagent (Cell Signalling, UK) were used to visualize proteins on C-
817 DiGit Chemiluminescent Blot Scanner (LI-COR Biosciences), according to the manufacturer's in-
818 structions. All the secondary antibody were from Cell Signalling, UK. Diagnostic proteins were used
819 for all the cellular fractions: GlnA (membrane protein), GarA (secreted and cytoplasmic protein),
820 RpfB (membrane and cell wall protein) and FtsZ (cytoplasmic protein).

821

822 **Cell culture and transfection conditions**

823 *D. discoideum* strain Ax2 was grown at 22°C in HL5c medium supplemented with 18 g/L Maltose
824 (Formedium, Norfolk, United Kingdom). For ectopic expression in *Dictyostelium*, Rv1813c family
825 coding sequences with *Dictyostelium* optimized codons (IDT, Integrated DNA Technologies, Inc.,
826 Coralville, Iowa 5224, USA) were cloned into pDXA-3C-myc (Manstein *et al.,* 1995). Plasmids were
827 linearized by ScaI and transfected by electroporation as described (Cornillon *et al.,* 2000). Clones
828 were selected in 5µg/mL G418.

829 HeLa (ATCC CRM-CCL-2) and HEK-293T (ATCC CRL-3216) cells were maintained in DMEM, high
830 glucose (Dulbecco's Modified Eagle Medium) containing 5% and 10% heat-inactivated foetal bo-
831 vine serum, respectively, and supplemented with GlutaMAX™ (Gibco Life Technologies), penicillin
832 (100 units/mL), and streptomycin (100 µg/mL). Transfections of HeLa cells were performed using
833 JetPEI™ transfection reagent (PolyPlus-Transfection, Ozyme, Saint Quentin, France), according to
834 the manufacturer. Cells plated one day before transfection were incubated with JetPEI™ -DNA com-
835 plexes (N/P=5), and after 5h the medium was changed. All assays were performed 48h post-trans-
836 fection.

837 For confocal microscopy analysis, HeLa cells were seeded on glass coverslips coated with 0.001%
838 poly-L-Lysine (# P4707, Sigma). For localization, Rv1813c family coding sequences with human
839 optimized codons were cloned into the mammalian expression vector pCI (a kind gift of Dr. Solange
840 Desagher, IGMM, Montpellier, France). Cells on glass coverslips were transfected in a 24-well cul-
841 ture plate and analyzed 48h later. For mitochondrial membrane potential, mitochondrial ROS and
842 oxidative stress studies, cells were transfected on 6-well culture plates. After 24h, resuspended
843 cells were pooled and plated either on glass coverslips for confocal microscopy or on 6-well culture
844 plates at a density of 2-3.10^5 cells/well for FACS analysis. For extracellular flux analysis, HeLa cells
845 seeded into five 100-mm tissue culture dishes were transfected with Rv1813c DNA cloned into
846 pMACS 4-IRESII vector (Miltenyi Biotec, France), allowing Rv1813c co-expression with a truncated
847 CD4 surface marker. After 24h, EDTA resuspended cells were pooled and CD4 positive cells se-
848 lected through magnetic cell sorting (MACS) as described below.
849
850 **Mitochondria isolation and biochemical treatments**
851 Mitochondria were isolated as described (Aubry *and* Klein, 2006). Briefly *Dictyostelium* cells were
852 washed in ice-cold buffer A (20 mM HEPES pH7, 1 mM EDTA, 250 mM Sucrose, proteinase inhib-
853 itors), resuspended at a cell density of 3x10^8 cells/mL, and broken with a ball bearing homogenizer
854 (8.02 mm bore, 8.002 mm ball; 20 strokes). Unbroken cells were removed by low speed centrifuga-
855 tion (5 min, 1500 g). The supernatant was next centrifuged for 15 min at 16,000 g. The pellet was
856 resuspended in buffer A and the centrifugation repeated to yield the enriched mitochondria fraction.
857 For further subcellular fractionation, this fraction was further centrifuged at 100,000 g for 1h. Triton
858 X-114 phase fractionation was performed as described (Bordier, 1981). Briefly, mitochondria were
859 incubated for 20 min at 4°C in 10 mM Tris-HCl pH7.4, 150 mM NaCl and 1% Triton X-114. Samples
860 were loaded on a 6% sucrose cushion, incubated at 30°C for 3 min for condensation, and centri-
861 fuged at 300 g for 3 min at room temperature. Supernatants were adjusted to 1% Triton X-114 and
862 the procedure repeated. Detergent and aqueous phases were analyzed by western blotting.
863 For Carbonate extraction of integral membrane proteins, mitochondria were incubated for 30 min
864 at 4°C in 0.1 M Na_2CO_3 pH11.5 and centrifuged for 30 min at 100,000 g as previously described
865 (Fujiki et al., 1982).Pellets were resuspended in buffer A. Proteins in resuspended pellets and su-
866 pernatants were precipitated with 15% TCA and resuspended in SDS page loading buffer. Integral
867 membrane proteins were recovered in the pellet, while soluble and peripheral proteins were present
868 in the supernatant. For high salt washes, intact mitochondria were incubated in 10 mM Tris-HCl
869 pH7.3, 250 mM Sucrose, 200 mM KCl and incubated for 30 min at 4°C. Mitochondria were then
870 centrifuged for 10 min at 16,000 g. Pellets and supernatants were treated as above. For proteinase
871 K digestions of mitochondrial peripheral membrane proteins, mitochondria in 20 mM HEPES pH7,
872 250 mM Sucrose, 100 mM KCl, 2 mM $MgCl_2$, 1mM KH_2PO_4 were incubated with 100 µg/mL protein-

873 ase K for 30 min at 4°C ± 1% Triton X100. Samples were then treated with TCA for protein precipi-
874 tation. To break selectively mitochondrial outer membranes, mitochondria were resuspended in
875 hypotonic buffer (2 mM HEPES pH7, 5 mM KCL, proteinase inhibitors) for 30 min at room temper-
876 ature. After centrifugation at 16,000 g for 10 min, pellets and supernatants were treated with TCA
877 as above.
878
879 **Immunocytochemistry**
880 *Dictyostelium* cells were applied on glass coverslips for 3h, and then fixed with 4% paraformalde-
881 hyde for 30 min, washed and permeabilized for 2 min in -20°C methanol. Cells were incubated with
882 the indicated antibodies for 1h, washed, and then stained with appropriate fluorescent secondary
883 antibodies for 30 min. After three washes, coverslips were mounted in Mowiol. Mammalian cells
884 were cultured on glass coverslips and fixed with 4% paraformaldehyde in phosphate-buffered sa-
885 line (PBS) for 20 min. Cells were washed in Tris-buffered saline (TS; 25mM Tris pH7.4, 150mM NaCl)
886 for 10 min. After permeabilization with 0.2% Triton X-100 in TS for 4 min, non-specific binding was
887 blocked with 0.2% gelatin from cold water fish skin (Sigma-Aldrich, France) in TS for 30 min. Cells
888 were incubated with primary antibodies in blocking buffer for 1h and were then washed 3 times
889 with 0.008% TritonX-100 in TS for 10 minutes. Cells were incubated for 30 minutes with Alexa-
890 Fluor-labelled secondary antibodies in blocking buffer. After rinsing in washing buffer, cell nuclei
891 were stained with 1 µg/ml Hoechst in TS for 5 minutes. Finally, coverslips were mounted with Pro-
892 long Gold Antifade (#P36934 Thermo Fisher Scientific). Slides were examined under a Leica TCS
893 SPE confocal microscope equipped with a 40X/1.15 or 63X/1.33 ACS APO oil-immersion objective
894 or a Zeiss LSM880 AiryScan confocal microscope equipped with a 40X/1.4 or 63x/1.4 Oil Plan-
895 apochromat DIC objective. Fluorescence images were adjusted for brightness, contrast and colour
896 balance by using the ImageJ software.
897
898 **Flow cytometry analysis of JC-1 and MitoSox stained cells**
899 For MitoSox red staining of HeLa cells, $2.5x10^5$ cells resuspended in CPBS buffer (PBS, 2.67 mM
900 KCl, 0.5 mM $MgCl_2$, 0.7 mM $CaCl_2$ and 0.1% glucose) were incubated in 5 µM MitoSox red. After
901 20 min at 37°C with shaking, cells were washed twice in CPBS buffer before FACS analysis. JC-1
902 staining of HeLa cells was made according to the manufacturer recommendations. Briefly, cells
903 cultured in 6-well culture plates ($2.5x10^5$/well) were incubated at 37°C in culture medium supple-
904 mented with 2 µM JC1. After 30min, cells were washed, resuspended in PBS, and directly analyzed
905 by flow cytometry. As positive control of JC-1 staining, 5 µM carbonyl cyanide m-chlorophenyl
906 hydrazone (CCCP) was added to cells during JC-1 cell incubation.
907
908 **MACS enrichment of CD4-Rv1813c transfected cells**

909 MACS enrichment of transfected cells was done with MACSelect Transfected Cell Selection kit
910 from Miltenyi Biotec, according to the supplier. Briefly, HeLa cells were transfected with empty
911 pMACS4-IRESII (as control) or pMACS4-IRESII-Rv1813c plasmids allowing expression of trun-
912 cated CD4 cell surface marker alone or in combination with Rv1813c respectively. After 24h, ~10^7
913 cells were washed, dissociated in ice cold PBS containing 5 mM EDTA, centrifuged at 200 g for 10
914 minutes at 4°C, and resuspended in 320 µl ice-cold de-gassed PBS supplemented with 0.5% bo-
915 vine serum albumin and 5 mM EDTA (PBE). Magnetic labelling of the transfected cells was achieved
916 by incubating cells with 80 µl of anti-CD4 coupled MACSelect MicroBeads on ice for 15 minutes.
917 Volume was adjusted to 2 ml with PBE and cells were subjected to magnetic separation using LS
918 column (Miltenyi Biotec) and MACS separator. After three washes with 3 ml of PBE, cells were
919 flushed out with 5 ml of PBE. To increase the purity of the magnetically labelled fraction, magnetic
920 separation was repeated once on a second LS column. After the final wash, cells were flushed out
921 with 5ml of cell culture medium, counted and seeded at a density of 1.85×10^4 cells/well on XF96 cell
922 culture microplates (Seahorse, Agilent Technologies, France) previously coated with 0.1mg/ml poly-
923 D-Lysine (#P7280, SIGMA) or on glass coverslips to evaluate the level of MACS enrichment of
924 transfected cells by immunofluorescence. Cells were incubated at 37°C and analyzed 24h later
925 using the Seahorse XF96 extracellular flux analyzer or by confocal microscopy.
926
927 **Extracellular flux analysis**
928 Cells plated the day before on XF96 cell culture microplates were washed with pre-warmed cell
929 culture medium 5h before analysis to eliminate dead cells. Extracellular Flux analysis was performed
930 using Seahorse XF Extracellular Flux analyzer, allowing simultaneous measurement of oxygen con-
931 sumption rate (OCR) and extracellular acidification rate (ECAR). Mitochondrial respiration and gly-
932 colytic function of the cells were measured using Cell Mito Stress Test Kit (#103015-100) and Cell
933 Glycolysis Stress Test Kit (#103020-100), respectively (Agilent Technologies, France). Cells were
934 incubated in Seahorse XF DMEM pH7.4 (#103575-100, Agilent) supplemented with 1 mM sodium
935 pyruvate, 2 mM glutamine and with 10 mM glucose (Cell Mito Stress Test Kit) or without glucose
936 (Cell Glycolysis Stress Test Kit) in a 37°C incubator without CO_2 for 1h prior to the assay. After
937 calibration and three initial measurements at baseline, different perturbing chemicals corresponding
938 to each kit were sequentially injected, and three successive measurements were taken after each
939 injection.
940
941 **Transmission electron microscopy**
942 MACS enriched cells on glass coverslips were successively fixed with 2.5% gluteraldehyde in 0.1
943 M cacodylate buffer pH 7.4, washed with cacodylate buffer, post-fixed in 1% osmium tetroxide in
944 cacodylate buffer, washed with distilled water, and finally incubated in 1% uranyl acetate. Dehy-
945 dration was performed through acetonitrile series. Samples were impregnated first in epon 118:

946 acetonitrile 50:50, and twice in 100% epon. After overnight polymerization at 60°C, coverslips were
947 detached by thermal shock with liquid nitrogen. Polymerization was then prolonged for 48h at 60°C.
948 Ultrathin sections of 70 nm were cut with a Leica UC7 ultramicrotome (Leica microsystems), coun-
949 terstained with lead citrate and uranyl acetate prepared in ethanol. Sections were observed in a
950 Jeol 1200 EXII transmission electron microscope. All chemicals were from Electron Microscopy
951 Sciences (USA) and solvents were from Sigma. Images were processed using the Fiji software.

A

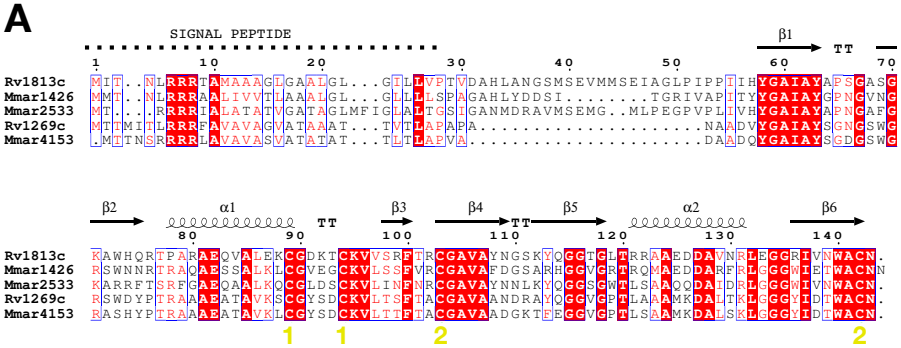
SIGNAL PEPTIDE
β1
TT
β2
α1
TT
β3
β4
TT
β5
α2
β6
Rv1813c
Mmar1426
Mmar2533
Rv1269c
Mmar4153
1
1
2
2

B

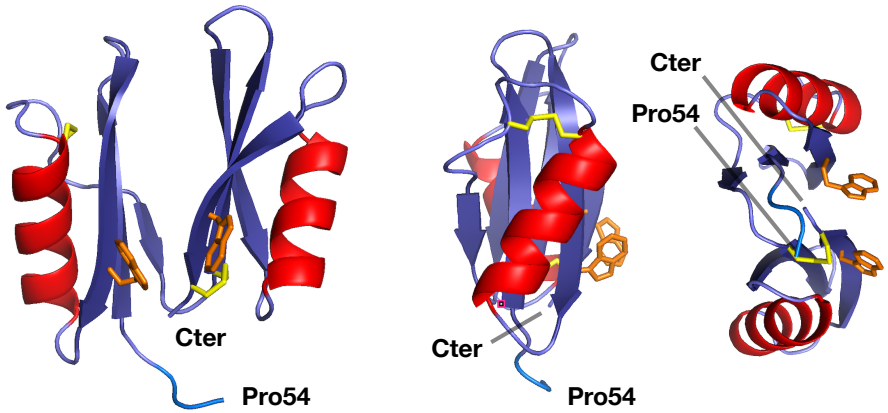
Cter
Pro54
Cter
Pro54
Cter
Pro54

Figure 2

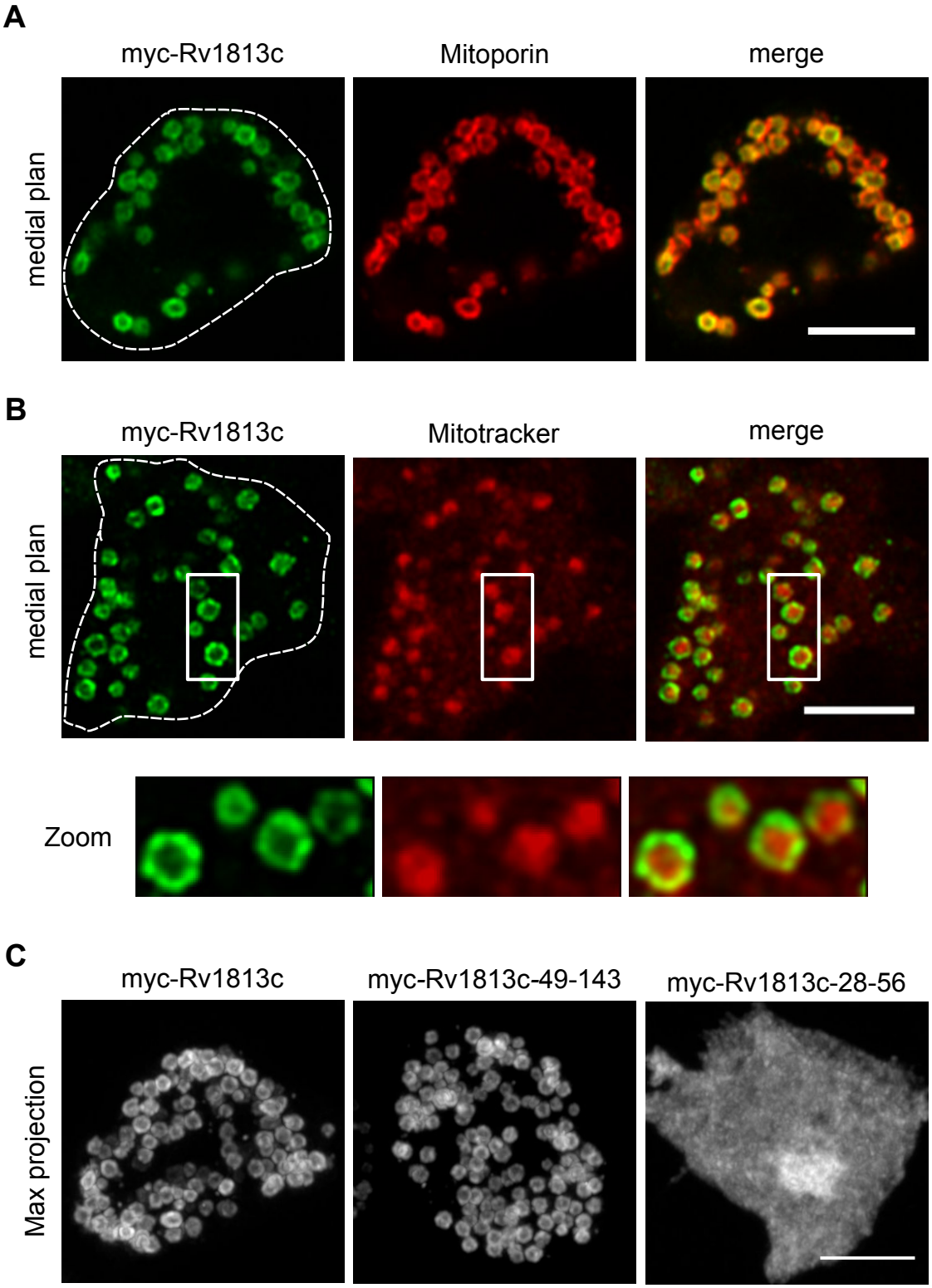
A
myc-Rv1813c
Mitoporin
merge
medial plan
B
myc-Rv1813c
Mitotracker
merge
medial plan
Zoom
C
myc-Rv1813c
myc-Rv1813c-49-143
myc-Rv1813c-28-56
Max projection

Figure 3

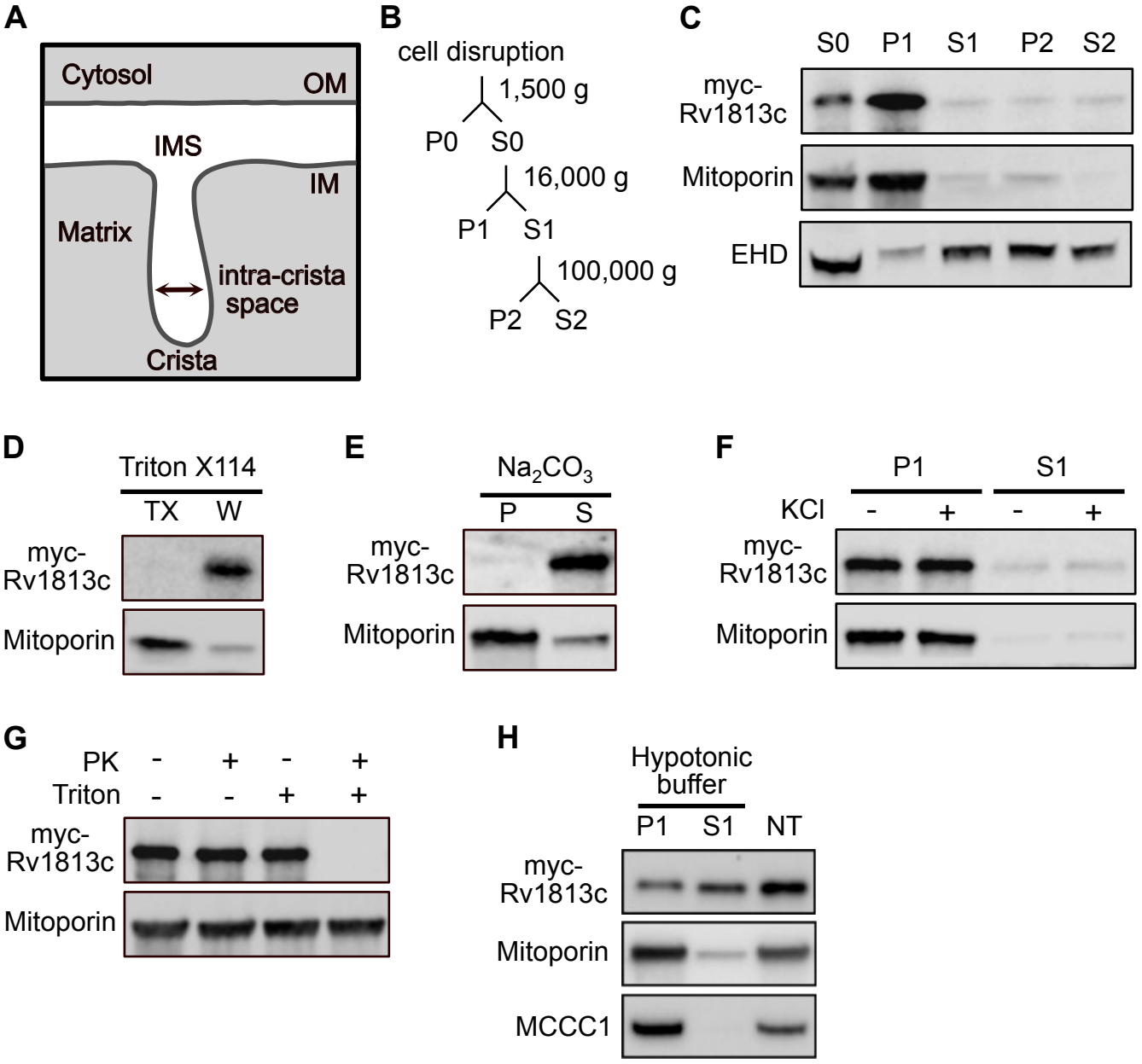
A
Cytosol
OM
IMS
IM
Matrix
intra-crista space
Crista
B
cell disruption
1,500 g
P0
S0
16,000 g
P1
S1
100,000 g
P2
S2
C
S0
P1
S1
P2
S2
myc-Rv1813c
Mitoporin
EHD
D
Triton X114
TX
W
myc-Rv1813c
Mitoporin
E
Na2CO3
P
S
myc-Rv1813c
Mitoporin
F
P1
S1
KCl
-
+
-
+
myc-Rv1813c
Mitoporin
G
PK
Triton
myc-Rv1813c
Mitoporin
H
Hypotonic buffer
P1
S1
NT
myc-Rv1813c
Mitoporin
MCCC1

Figure 4

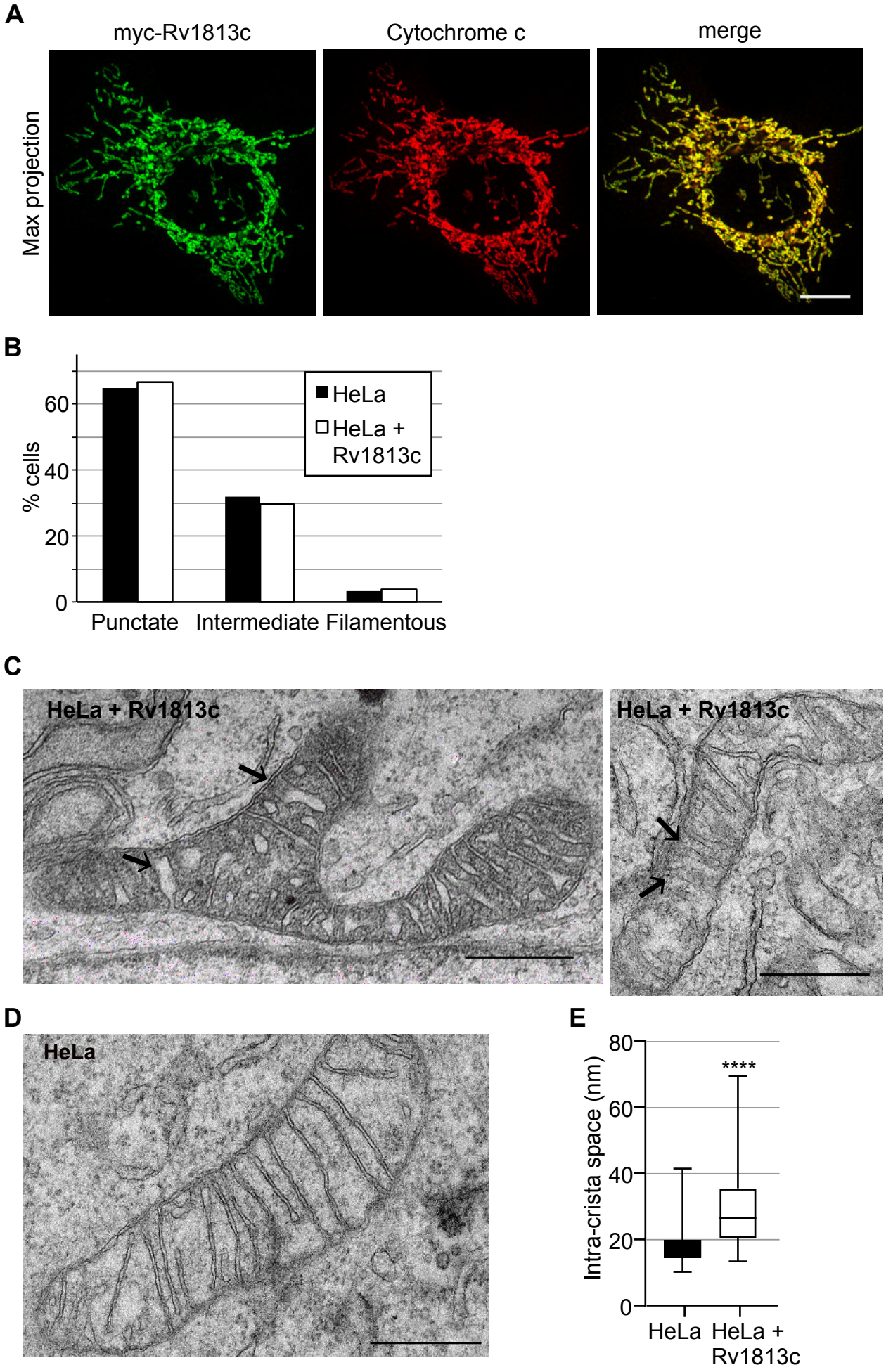
A
myc-Rv1813c
Cytochrome c
merge
Max projection
B
% cells
60
40
20
0
HeLa
HeLa + Rv1813c
Punctate
Intermediate
Filamentous
C
HeLa + Rv1813c
HeLa + Rv1813c
D
HeLa
E
Intra-crista space (nm)
80
60
40
20
0
****
HeLa
HeLa + Rv1813c

Figure 5

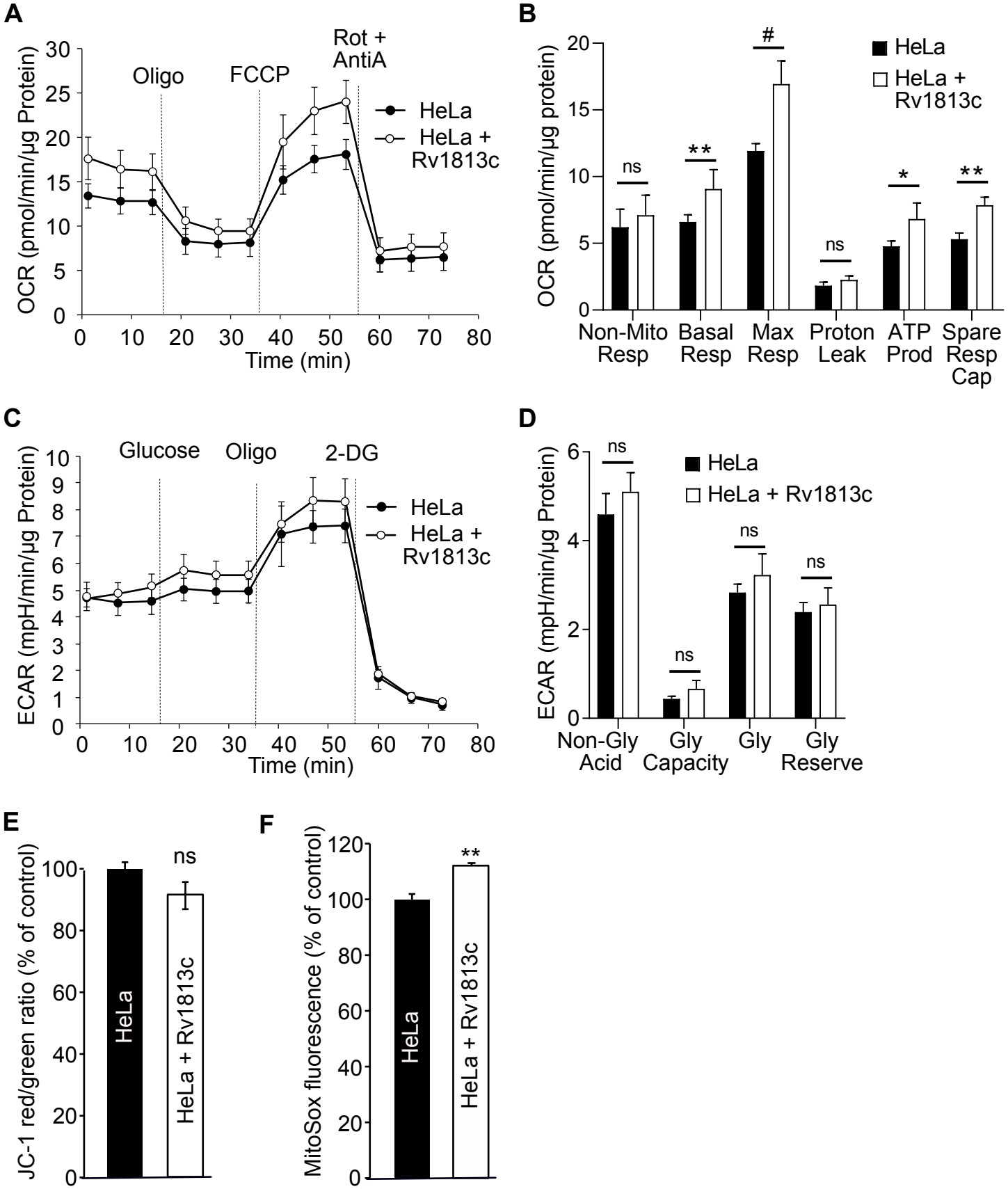
A
OCR (pmol/min/µg Protein)
Oligo
FCCP
Rot + AntiA
HeLa
HeLa + Rv1813c
Time (min)
B
OCR (pmol/min/µg protein)
HeLa
HeLa + Rv1813c
ns
**
#
ns
*
**
Non-Mito Resp
Basal Resp
Max Resp
Proton Leak
ATP Prod
Spare Resp Cap
C
ECAR (mpH/min/µg Protein)
Glucose
Oligo
2-DG
HeLa
HeLa + Rv1813c
Time (min)
D
ECAR (mpH/min/µg Protein)
HeLa
HeLa + Rv1813c
ns
ns
ns
ns
Non-Gly Acid
Gly Capacity
Gly
Gly Reserve
E
JC-1 red/green ratio (% of control)
ns
HeLa
HeLa + Rv1813c
F
MitoSox fluorescence (% of control)
**
HeLa
HeLa + Rv1813c

Figure 6

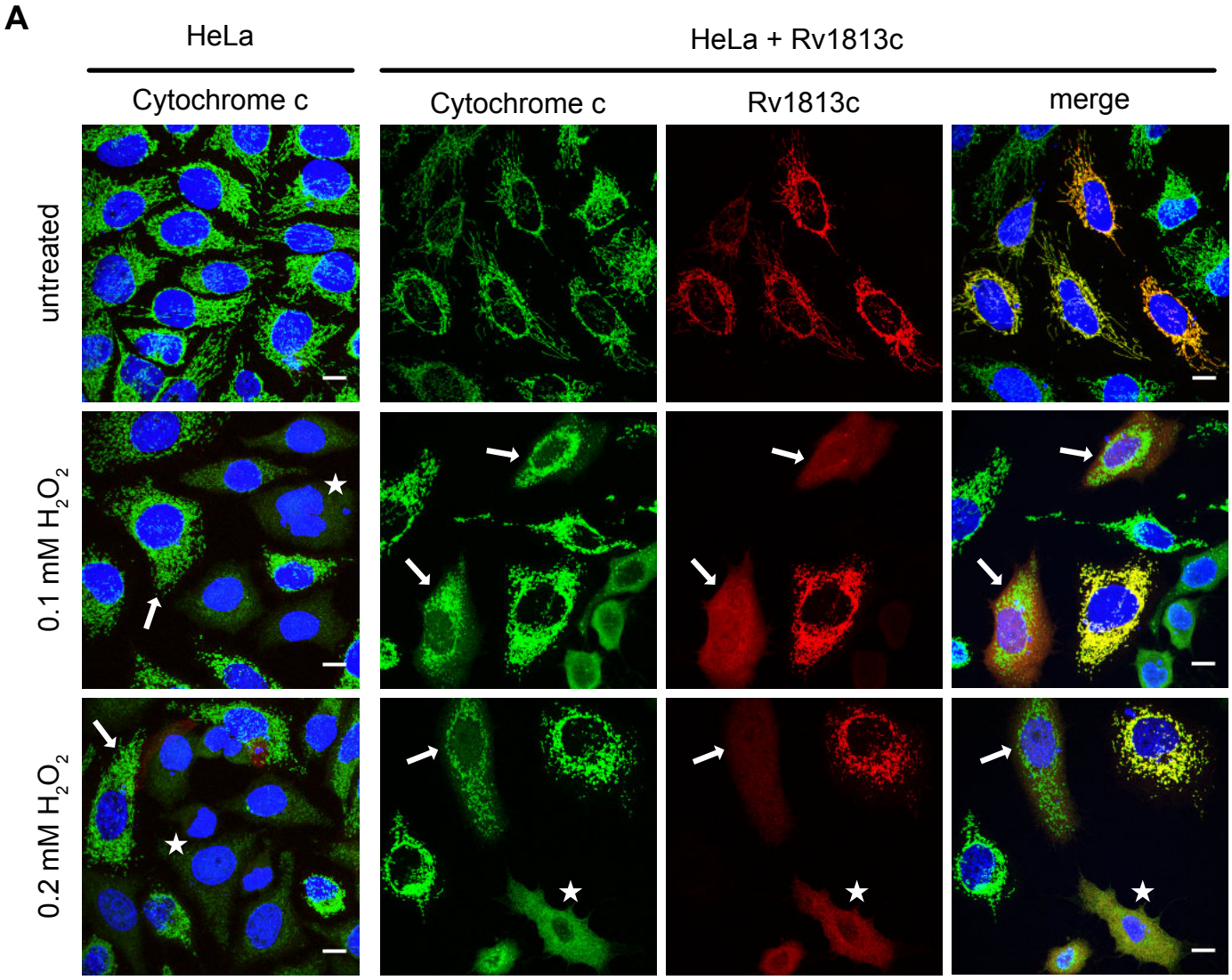
A
HeLa
HeLa + Rv1813c
Cytochrome c
Cytochrome c
Rv1813c
merge
untreated
0.1 mM H_2O_2
0.2 mM H_2O_2

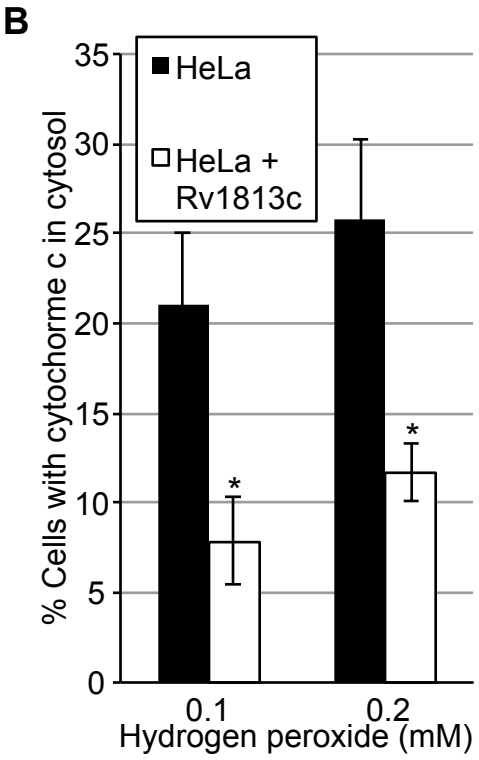
B
HeLa
HeLa + Rv1813c
% Cells with cytochorme c in cytosol
0
5
10
15
20
25
30
35
*
*
0.1
0.2
Hydrogen peroxide (mM)

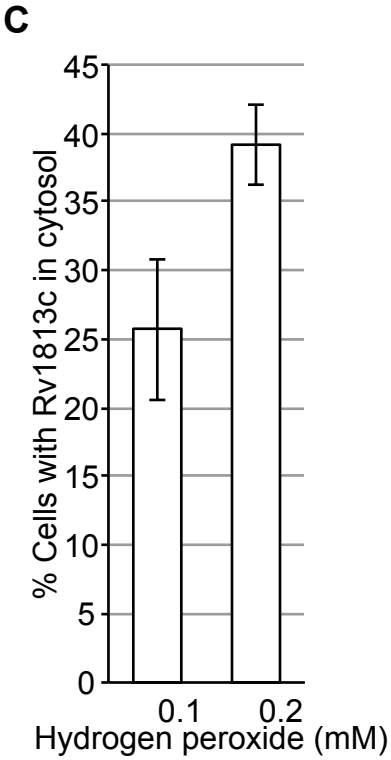
C
% Cells with Rv1813c in cytosol
0
5
10
15
20
25
30
35
40
45
0.1
0.2
Hydrogen peroxide (mM)

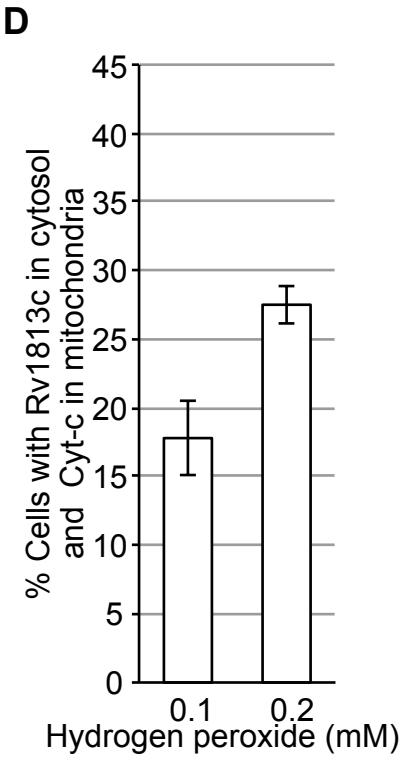
D
% Cells with Rv1813c in cytosol and Cyt-c in mitochondria
0
5
10
15
20
25
30
35
40
45
0.1
0.2
Hydrogen peroxide (mM)

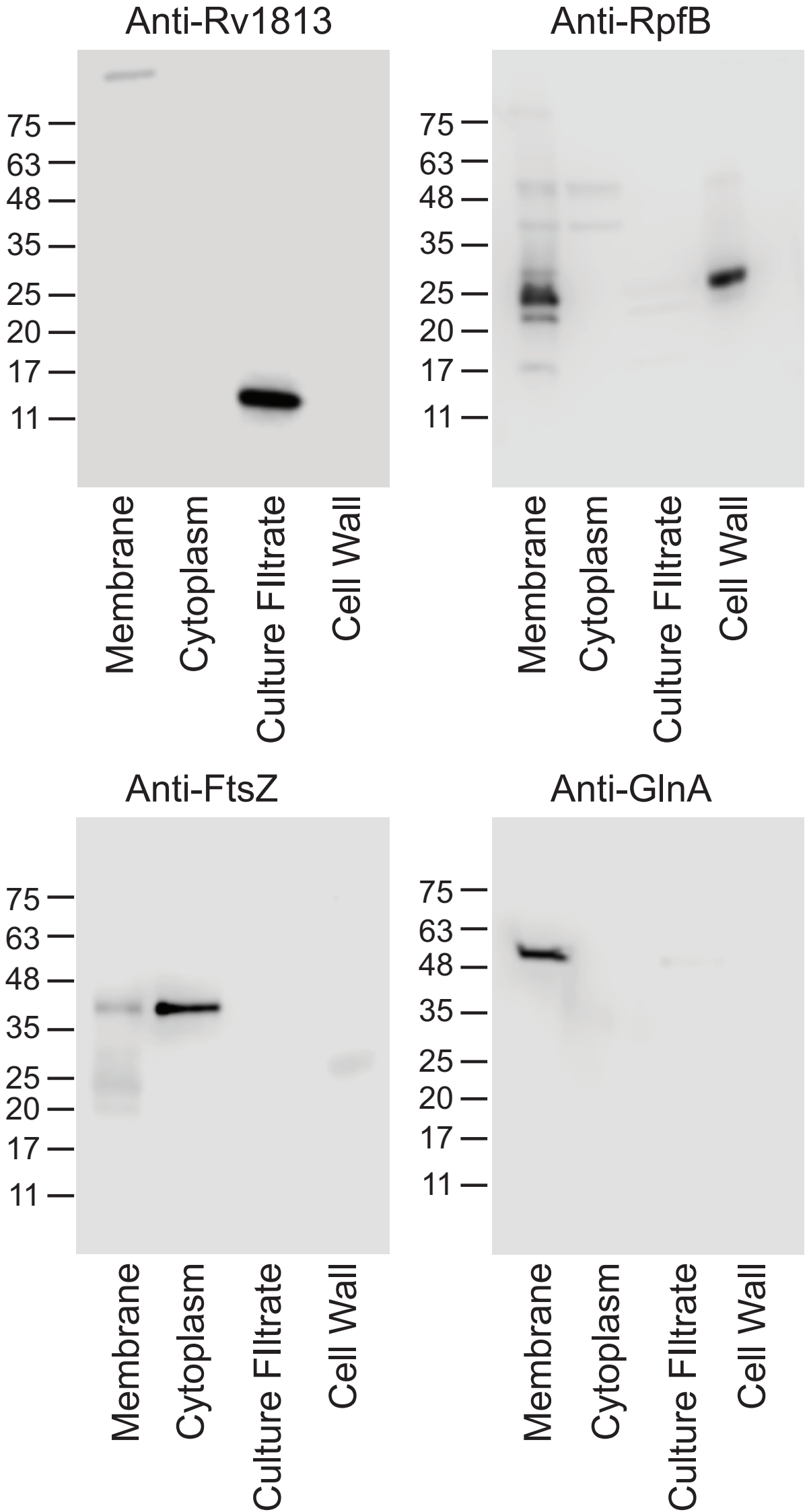
Anti-Rv1813
75
63
48
35
25
20
17
11
Membrane
Cytoplasm
Culture FIltrate
Cell Wall
Anti-RpfB
75
63
48
35
25
20
17
11
Membrane
Cytoplasm
Culture FIltrate
Cell Wall
Anti-FtsZ
75
63
48
35
25
20
17
11
Membrane
Cytoplasm
Culture FIltrate
Cell Wall
Anti-GlnA
75
63
48
35
25
20
17
11
Membrane
Cytoplasm
Culture FIltrate
Cell Wall

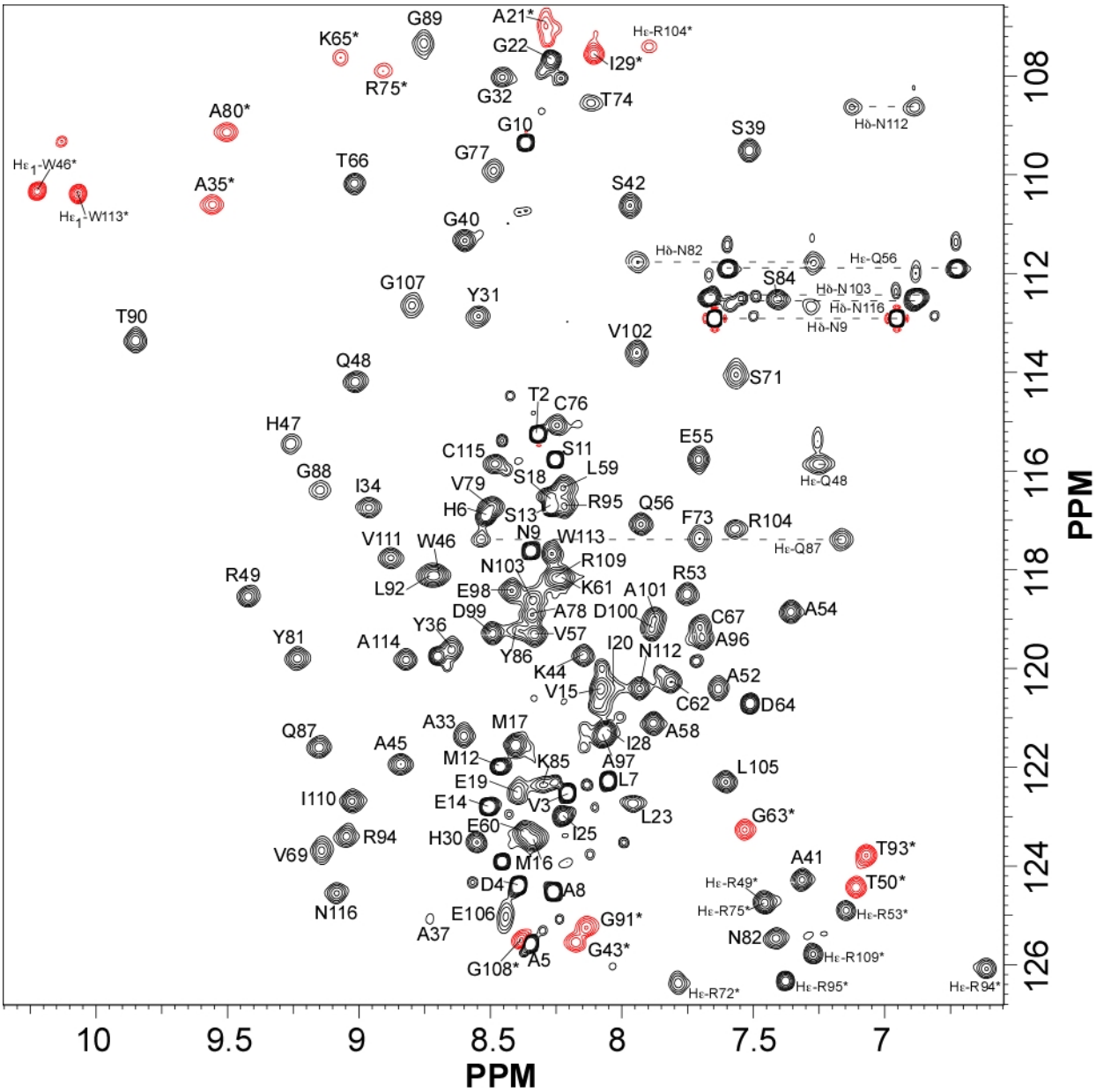
G89
A21*
Hε-R104*
K65*
G22
I29*
R75*
G32
T74
A80*
G10
S39
Hδ-N112
Hε1-W46*
T66
G77
A35*
S42
Hε1-W113*
G40
Hδ-N82
Hε-Q56
S84
Hδ-N103
Hδ-N116
Hδ-N9
G107
Y31
T90
V102
Q48
S71
T2
C76
H47
E55
C115
S11
L59
G88
S18
Hε-Q48
I34
V79
R95
Q56
H6
S13
F73
R104
V111
W46
N9
W113
Hε-Q87
R109
R49
N103
R53
L92
E98
K61
A101
A54
D99
A78
D100
C67
Y36
V57
A96
Y81
A114
Y86
I20
N112
K44
A52
V15
C62
D64
A33
M17
Q87
A58
A45
M12
K85
I28
A97
L105
E19
L7
I110
E14
V3
L23
G63*
E60
R94
H30
I25
V69
M16
A41
T93*
D4
A8
Hε-R49*
T50*
N116
E106
Hε-R75*
Hε-R53*
G91*
A37
N82
G43*
G108*
A5
Hε-R109*
Hε-R72*
Hε-R95*
Hε-R94*
108
110
112
114
116
118
120
122
124
126
PPM
10
9.5
9
8.5
8
7.5
7
PPM

Figure S3

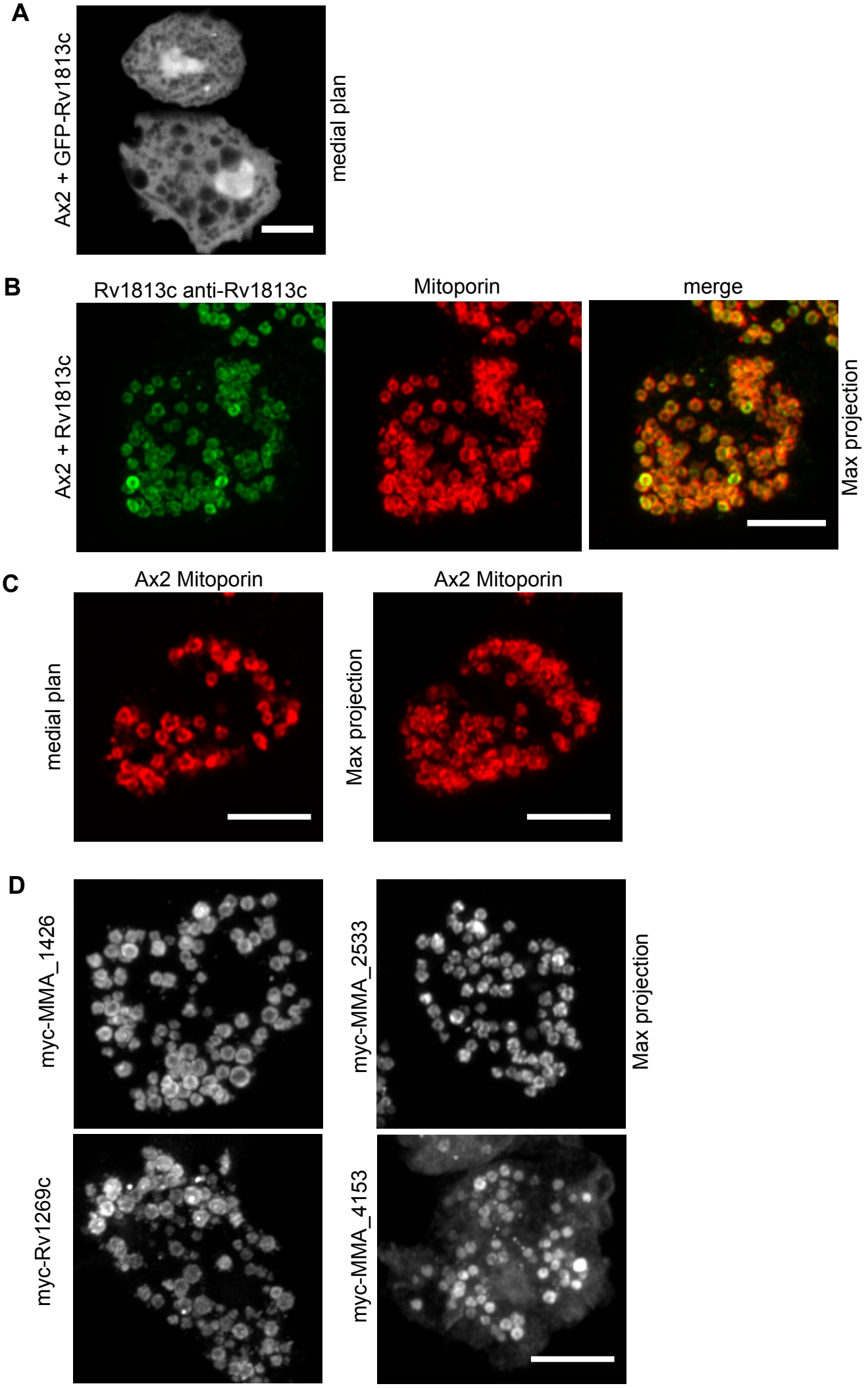
A
Ax2 + GFP-Rv1813c
medial plan
B
Rv1813c anti-Rv1813c
Mitoporin
merge
Ax2 + Rv1813c
Max projection
C
Ax2 Mitoporin
Ax2 Mitoporin
medial plan
Max projection
D
myc-MMA_1426
myc-MMA_2533
Max projection
myc-Rv1269c
myc-MMA_4153

Fig. S4

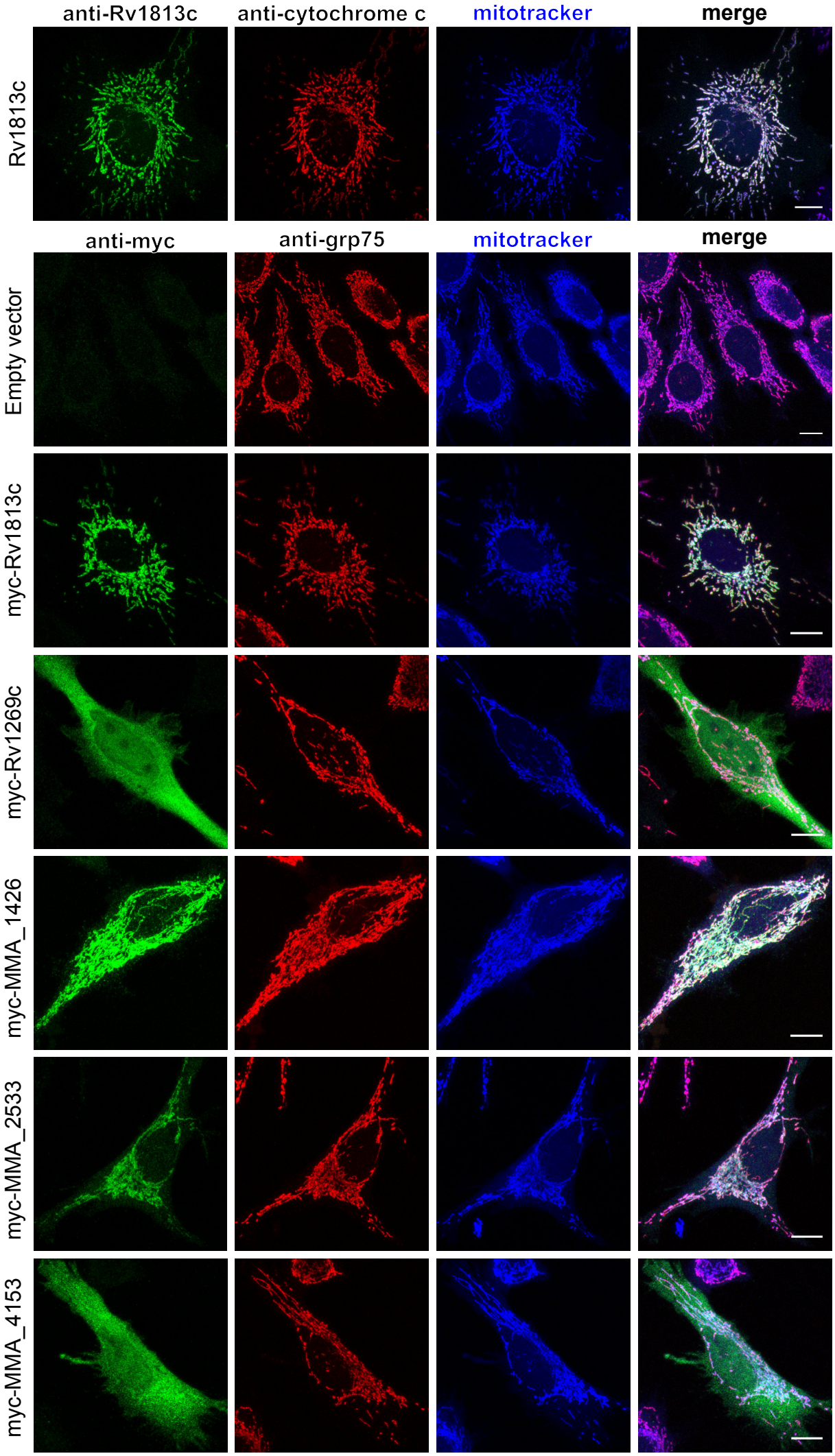
anti-Rv1813c
anti-cytochrome c
mitotracker
merge
Rv1813c
anti-myc
anti-grp75
mitotracker
merge
Empty vector
myc-Rv1813c
myc-Rv1269c
myc-MMA_1426
myc-MMA_2533
myc-MMA_4153

Fig. S5

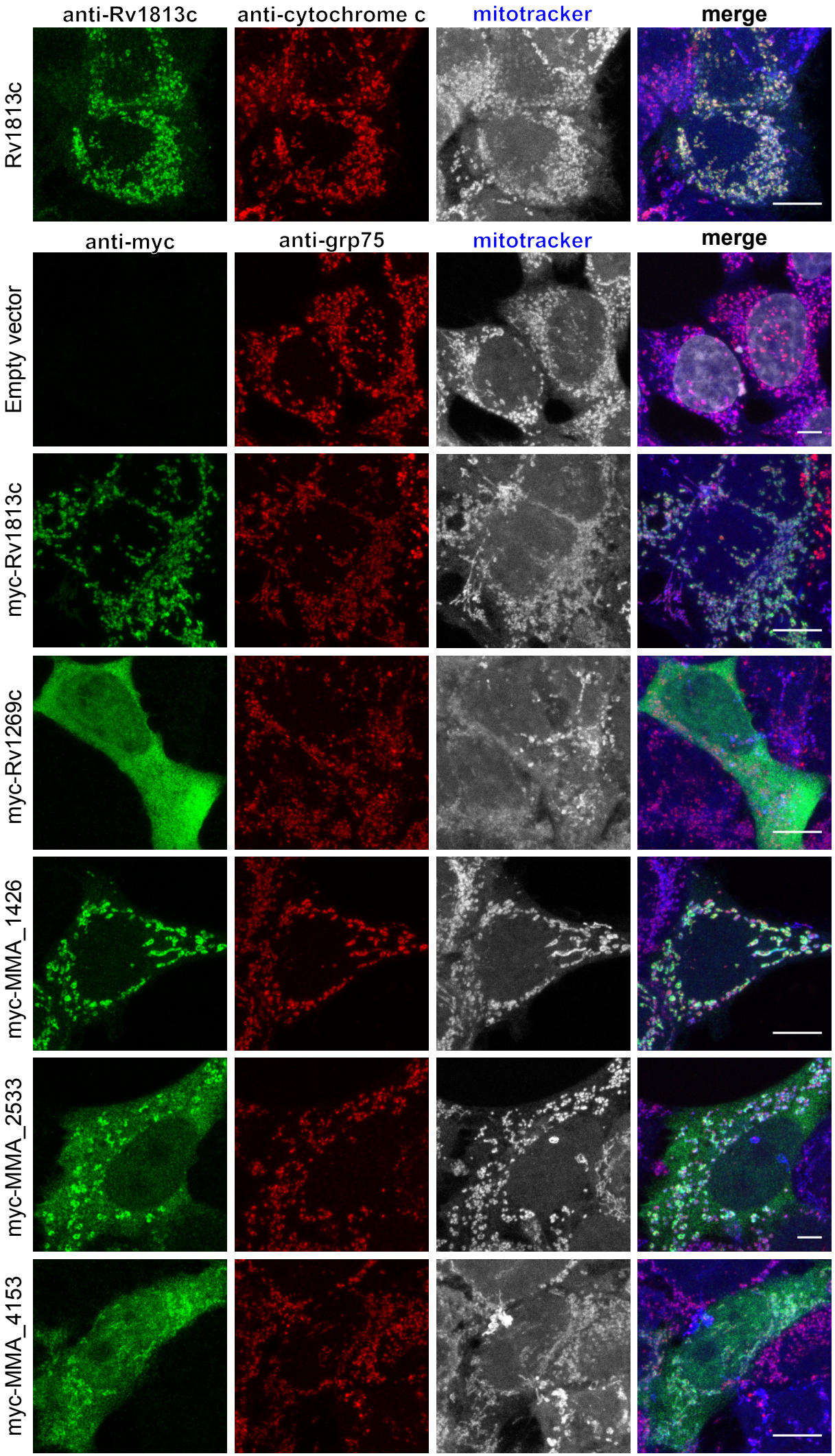
anti-Rv1813c
anti-cytochrome c
mitotracker
merge
Rv1813c
anti-myc
anti-grp75
mitotracker
merge
Empty vector
myc-Rv1813c
myc-Rv1269c
myc-MMA_1426
myc-MMA_2533
myc-MMA_4153
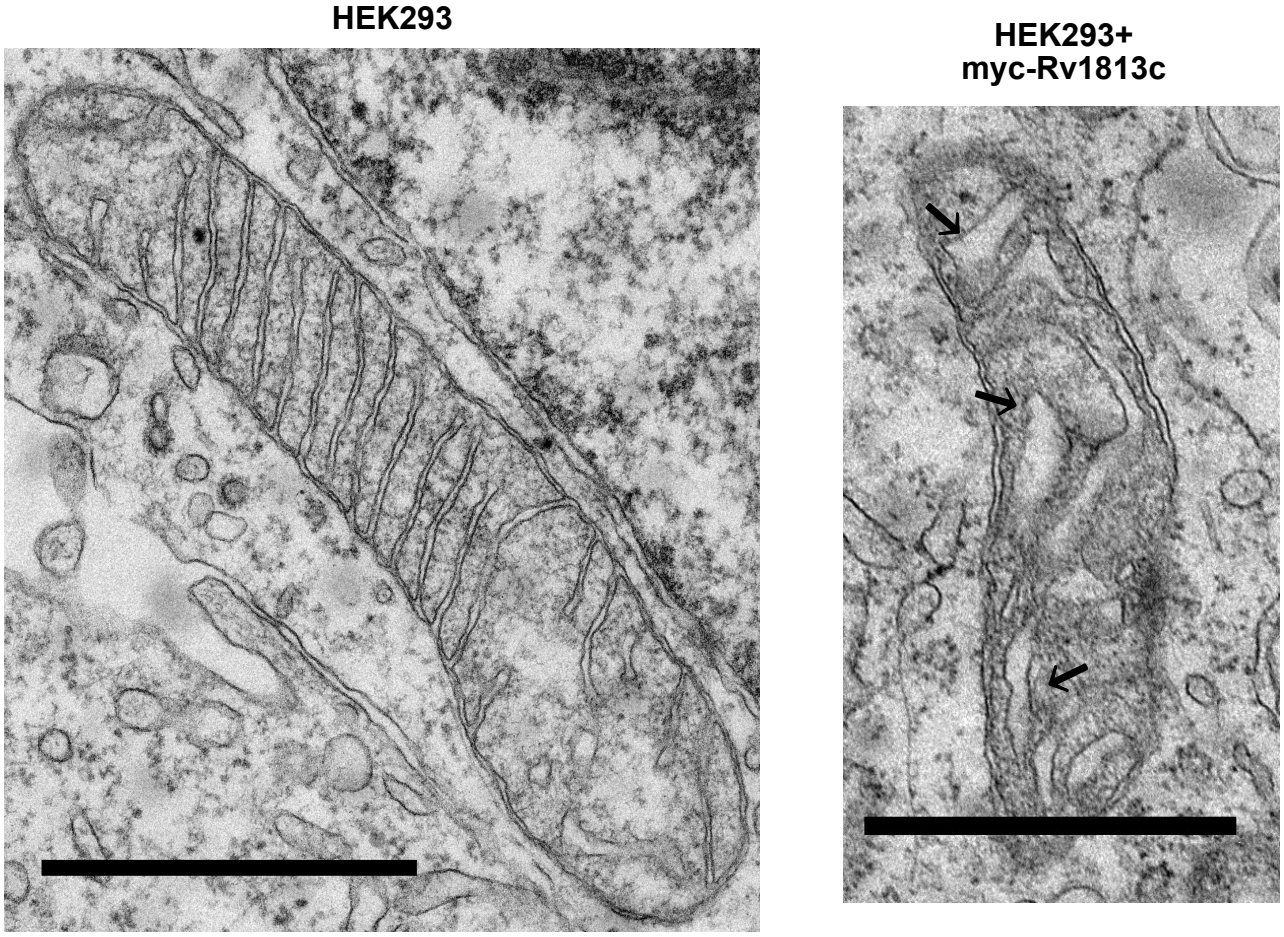
Figure S6